R. & M. No. 3463

R. & M. No. 3463

MINISTRY OF TECHNOLOGY

AERONAUTICAL RESEARCH COUNCIL
REPORTS AND MEMORANDA

A New Two-Parameter Family of Mean Velocity Profiles for Incompressible Turbulent Boundary Layers on Smooth Walls

By B. G. J. Thompson, Ph.D.

LONDON: HER MAJESTY'S STATIONERY OFFICE
1967
PRICE £1 15*s.* 0*d.* NET

A New Two-Parameter Family of Mean Velocity Profiles for Incompressible Turbulent Boundary Layers on Smooth Walls

By B. G. J. Thompson, Ph.D.

COMMUNICATED BY PROFESSOR W. A. MAIR, UNIVERSITY OF CAMBRIDGE

Reports and Memoranda No. 3463*
April, 1965

Summary.

The combination of two universal functions, representing the effects of the wall and of the 'intermittency' in the other region, has been used to construct a new profile family. Charts are presented from which complete profiles and values of c_f, and $H_{\delta-\delta^*}$ may readily be obtained for given values of H and R_θ. Comparisons with measured profiles are very satisfactory for a wide range of local and of upstream conditions, whilst the skin-friction values should be rather more reliable than those of the well-known Ludwieg and Tillmann relationship, especially when R_θ is less than 2000 or H exceeds 2·0.

In severe adverse pressure gradients the 'universal' wall law breaks down and an estimate is given for the range of pressure gradient beyond which no two-parameter family is likely to be satisfactory.

LIST OF CONTENTS

*Replaces A.R.C. 26 830.

---

1. *Introduction.*

1.1. *The Use of Velocity Profile Families in Calculation Methods*

In order to carry out turbulent boundary-layer calculations in the normal way it is necessary to relate the various quantities appearing in the basic equations to the usual variables H and R_θ, and in principle also to parameters such as the local pressure gradient parameter Γ_1, depending on the local boundary conditions, although the use of such additional parameters does not, so far, appear to have been thought necessary. Now, whilst it is possible in each case to determine these relationships directly from measured velocity profiles as, for instance, was done in the case of the single-parameter relationships, $H_{\delta-\delta^*}$ *vs.* H (Head[13]), H *vs.* H_ε (Fernholz[11]), η *vs.* H (Gruschwitz[12], Kehl[16]), it is very much more difficult to repeat this process if two or more independent variables are involved. In the latter case, therefore, the characteristics of a number of measured velocity profiles are summarised by means of a suitable profile family (for example, Rotta[26]; Kawasaki[15], using the results of Coles[5], and Spence[35]), as this allows the necessary interpolation between the scattered experimental values of H and R_θ. Contour plots can therefore be constructed more accurately, although these might not be used directly in calculations but could be represented by a matrix of numbers or approximated by a suitable analytic expression as, for example, the skin-friction relationship of Ludwieg and Tillmann[20].

1.2. *The Use of Two Parameters.*

The determination of a profile family is thus of some practical importance as no single-parameter representation has yet been discovered that will adequately describe explicit profile shapes over more than a small part of the Reynolds number range covered by the existing experiments. As will be shown later in this report, the neglect of the effects of Reynolds number variation was responsible for the striking disagreement between measured profiles obtained in the equilibrium layers of Clauser[2] and the predic-

tions given, for the same H values, by the singly-infinite profile family of von Doenhoff and Tetervin[8]. Clauser's figure is reproduced here as Fig. 1. Moreover, it is now generally accepted on physical grounds that the turbulent layer can only be described in terms of a minimum of two regions (inner and outer) each having rather different characteristics (*see* Townsend[42], and Rotta[26], for example), and this necessitates the use of at least two independent parameters to define the velocity profile.

1.3. *The Choice of the Basis for the New Profile Family.*

The division of the layer into inner and outer regions also allows the skin friction to be related to the overall profile shape and has formed the basis of a number of two-parameter models, four of which were considered for building up the profile family required in the development of a new calculation method (Thompson[39]). Each of these made use of an assumed 'universal' wall law having the conventional semi-logarithmic fully turbulent portion (with only slightly different values of the coefficients A, B being assumed by the different authors) but with the following different procedures for obtaining the form of the outer profile:

(a) When considering equilibrium layers, Clauser[3] and Townsend [42] assumed a constant eddy viscosity in the outer region in order to complete the reduction of the boundary layer equations to an ordinary differential form. The complete velocity distribution was obtained by matching this solution for the outer profile to the 'universal' wall region profile. These velocity distributions could have been used in non-equilibrium conditions if they had been specified afresh in terms of H and R_θ.

(b) The assumption of a linear shear stress variation in the outer region, combined with the use of the Prandtl momentum transfer theory and a constant mixing length, was used by Ross[24] to give a velocity defect law.

(c) Coles[5] analysed many experimental velocity profiles, obtaining good correlations for his apparently universal 'Wake law', which describes the departure of the profile, in the outer region, from the 'universal' wall law. Rotta[26] describes some earlier assumptions for the outer profiles made by Ross and Robertson, and by himself, which were along similar lines.

(d) Sarnecki[28] recognised the fundamentally intermittent nature of the turbulent flow in the outer region of the boundary layer and succeeded in obtaining an apparently universal correlation analogous to the 'Wake law' in some respects.

(a) and (b) were rejected as only a few direct comparisons with measured profiles were shown and even these were not well represented in detail. Moreover, (b) could not overlap the inner law and required a large (unknown) transition region to complete the description of the profile.

In spite of the larger amount of data very carefully considered by Coles, it was decided to use Sarnecki's method (d) in preference to (c) as the basis for the new profile family, pricipally because of the ease with which the effects of suction or blowing could be incorporated at a later stage. This was especially important as the final aim of the present author's work was the establishment of a method of calculating the development of turbulent layers with suction, and in connection with this it should be remembered that Black and Sarnecki[1] had already encountered difficulties in attempting to use the 'Wake law' in conditions of transpiration. However, the present paper deals only with profiles on smooth solid walls and the new model should be at least as accurate as that of Coles in these conditions. Finally, the presentation of charts of y/θ contours in the H *vs.* $\log_{10} R_\theta$ plane for a range of values of $\frac{u}{U_1}$ (Figs. 6a to 6n), allows the direct comparison of the new family with experiment whereas the alternative families have yet to be presented in an explicit fashion.

2. *The Intermittent Structure of the Turbulent Boundary Layer*

2.1. *Qualitative Physical Features.*

The measurements of Corrsin and Kistler[7] and others showed that the overall time-mean boundary-layer characteristics were the result of time-sharing between potential and turbulent flow in the outer

region. The body of turbulent fluid possessing mean and fluctuating vorticity extends, at any instant, from the wall to an outer boundary surface or turbulence 'front', beyond which lies the potential flow undergoing only pressure and velocity variations. The irregular nature of the 'front' is shown clearly by Figs. 2a and b, which are short time-exposure photographs† of a smoke-filled boundary layer developing in zero pressure gradient. Illumination is provided by a parallel beam of light directed normal to the surface and having only a small (spanwise) width so as to pick out a streamwise cross-section of the instantaneously three-dimensional turbulent core. The intermittent region is seen to consist of streamers of smoke-filled turbulent fluid, separated by smokeless regions of potential flow, and rising out of a region of continuous turbulence adjacent to the wall.

The extent of the turbulent region is quite sharply defined in terms of the level of vorticity fluctuations, as the vorticity spreads into the potential flow by means of viscous diffusion which is a short-range influence. However, the definition in terms of velocity fluctuation is much poorer, as hot-wire measurements show (for example, Klebanoff[17]), because momentum can be transferred by means of longer range pressure forces, giving rise to irrotational velocity variations outside the turbulence 'front'.

2.2. *Quantitative Description.*

In order to describe quantitatively the behaviour of the outer region of the turbulent layer it is necessary to be able to relate the overall time-mean properties to their mean values taken over the times for which the flow is turbulent, or potential, at any position. These mean values will be denoted by the suffices t and p, respectively. It is also necessary to know the properties of the distorted outer surface of the turbulent layer, in particular, the fraction of the time for which the flow is turbulent at any height (y) from the surface, is an important characteristic. This is called the 'intermittency factor' (γ), and represents an integrated effect of the passage of the bulges in the turbulence 'front'.

The mean velocity distribution is of particular importance and may be written in terms of the properties of the turbulent and irrotational flows.

That is,

$$u = \gamma u_t + (1-\gamma)u_p, \tag{1}$$

where u_t is the mean velocity taken over 'time turbulent', and u_p is the mean velocity taken over 'time potential'.

The intermittency factor was first measured by Corrsin[6] for a round jet, and then by Townsend[41] for a plane wake. Later, measurements for the zero pressure gradient boundary layer were made by Corrsin and Kistler[7] for a rough wall, and by Klebanoff[17] for a smooth wall. These distributions all have a characteristic approximate anti-symmetry about the $\gamma = 0{\cdot}5$ position, with boundary conditions of $\gamma \to 0$, $y \to \infty$; $\gamma = 1$, $y = 0$. The result due to Klebanoff is shown in Fig. 3 in terms of $\frac{y}{\delta_K}$ where δ_K is the choice of boundary-layer thickness made by Klebanoff.

That is,

$$\gamma_K = \gamma_K\left(\frac{y}{\delta_K}\right). \tag{2}$$

Measurements were made for only one station at which $H = 1{\cdot}34$, $R_\theta = 7400$.

Direct measurements of the distributions of $u_t(y)$ and $u_p(y)$ have not yet been made, and there is some difference of opinion, in the literature, regarding the possible assumptions for u_p.

---

†For which the writer is indebted to Mr. S. A. M. Thornley.

Stewart[36] showed that there could be a variation in the mean velocity of the potential flow due to the presence of the turbulent layer and wrote

'It is pointed out that, contrary to a statement of Corrsin and Kistler[7], it is possible for the vorticity-free fluid between bulges of turbulent fluid to partake of the mean velocity of the turbulent fluid'.

Corrsin and Kistler had stated that,

'... the mean velocity everywhere in the potential part of the flow must be constant and equal to that at infinity ...'.

Townsend[42] also recognised that this statement was not well founded, because the irrotational fluid will be affected by the pressure field of the larger turbulent motions.

It should be noticed, however, that if a pitot-tube having poor directional sensitivity is placed in the intermittent region the full total pressure is picked up in the potential flow. Consequently, if the static pressure is assumed to be equal to the value at the wall, or in the external stream, then the pitot-tube will receive a contribution to its overall mean reading as if $u_p = U_1$ everywhere. Hence the simple assumption $u_p = U_1$ may be as accurate as is justified by the nature of the mean velocity profile data available.

The distribution of u_t is more difficult to describe and this formed the main problem in attempting to use a profile model based upon the concept of intermittent flow.

3. *The New Profile Family.*

3.1. *The 'Intermittency' Hypothesis of Sarnecki.*

The marked similarity between the distributions of turbulence intensity (and shear stress) in the wall regions of fully developed pipe flow and in the constant pressure turbulent boundary layer, was shown by Schubauer[30] to apply to much of the outer region if only those parts of the boundary layer that were instantaneously turbulent were considered. This analogy between the properties of the fully turbulent flow in a boundary layer and those of pipe flow, led Sarnecki[28] to propose that the mean velocity over 'time turbulent' (u_t) of the turbulent fluid in the boundary layer, should be represented by the 'universal' wall law profile $\frac{u}{U_\tau} = f\left(\frac{U_\tau y}{\nu}\right)$ having a semi-logarithmic portion for $\frac{U_\tau y}{\nu} \geqslant 60$. The complete profile is shown in Fig. 4, where the blending region profile of van Driest[9] has been used and Sarnecki's chosen values for constants (A and B) in the logarithmic law

$$\frac{u}{U_\tau} = A + B \log_{10} \frac{U_\tau y}{\nu}, \tag{3}$$

have been retained for the present application, so that $A = 5{\cdot}4$; $B = 5{\cdot}5$ and hence,

$$u_t = U_\tau \left[5{\cdot}4 + 5{\cdot}5 \log_{10} \frac{U_\tau y}{\nu} \right] . \tag{4}$$

Sarnecki's complete expression for the overall mean velocity distribution was obtained by assuming that the potential flow outside the turbulence 'front' had a mean velocity, over 'time potential', equal to the local free-stream velocity, and that any real blending region between the assumed velocity distributions either side of the turbulence 'front' could be replaced by a discontinuous velocity change.

That is,

$$u_p = U_1 , \tag{5}$$

and hence, from equation (1),

$$u = \gamma_s u_t + (1 - \gamma_s) U_1 , \tag{6}$$

where γ_s is the 'intermittency' function relating to the equivalent turbulence front position of the model flow and is not necessarily the same as the real intermittency (γ_K for zero pressure gradient), as it is to be expected that the real velocity variation will include a finite blending region between the fully turbulent core and the undisturbed free stream.

3.2. *The Inner Region Velocity Distribution.*

Two difficulties arise in the use of the 'universal' wall law and these will affect not only the present approach but all existing alternative profile families.

(i) If the longitudinal pressure gradient and the rate of flow development locally are such as to cause a sufficient variation of shear stress through the wall region, then departures from the simple 'universal' form will occur, at a value of $\frac{U_\tau y}{\nu}$ which depends on the severity of the stress variation. Consequently, the range of conditions for which the simple universal form, especially the fully turbulent portion [equation (3)], is accurate enough for the practical purposes of describing the inner velocity distribution and relating c_f to the overall profile shape, must be found from experiment in order to find the range of conditions over which the two-parameter representation is sufficiently accurate. This aspect is dealt with, in more detail, following the comparison of the new family with experiment.

(ii) Even in conditions where the stress variation in the inner region is small and a definite logarithmic portion appears, the experiments in which skin friction has been determined directly give rise to a wide range of A and B values, and consequently, before the profile family can be constructed, some estimate of the best mean values of these coefficients must be made.

Sarnecki allowed for the uncertainty in the choice of a 'best-fit' mean line to any given set of measured values plotted in coordinates $\frac{u}{U_1}$ *vs.* $\log_{10}\frac{U_1 y}{\nu}$. by assuming that all profiles must pass through the point $\frac{u}{U_\tau} = 16{\cdot}4, \frac{U_\tau y}{\nu} = 100$. This assumes the relationship

$$A+2B = 16{\cdot}4, \tag{7}$$

which is the average of existing estimates, based on the values of A and B given by Ludwieg and Tillmann[20], Clauser[2], Schultz-Grunow[33], Coles[4], and Dutton[10].

The semi-logarithmic part of the profile may be written as

$$\frac{u}{U_1} = M+N\log_{10}\frac{U_1 y}{\nu}, \tag{8}$$

where

$$M = \left(\frac{A}{B}-\log_{10}B\right)N+N\log_{10}N, \tag{9}$$

and $N = \frac{BU_\tau}{U_1}$, are constants for a particular line chosen to fit a given set of experimental points.

Hence values of A and B may be varied, keeping $\left(\frac{A}{B}-\log_{10}B\right)$ constant and also satisfying equation (7), if the value of c_f is revised from the original values given by the particular author concerned. Following such a readjustment, Sarnecki then took the average values

$$A = 5{\cdot}4; B = 5{\cdot}5,$$

which, as mentioned above, have been used in the present investigation.

Sarnecki's technique may be criticised as it considers neither the relative reliabilities of the skin-friction measurements that were made, nor the physical details of the various flows. That is, he does not weight the different estimates of A and B, or consider the possibility of variations due to the presence of a real physical non-similarity.

Now, Ross[25] has reanalysed the pipe measurements of Nikuradse to obtain the average values $A = 5{\cdot}6$; $B = 5{\cdot}6$. However, a wide range of values are reported for the zero pressure gradient boundary layer, of which the extremes are given by Smith and Walker[34] who find $A = 7{\cdot}15$; $B = 5{\cdot}0$ for their larger Reynolds numbers, and Schultz-Grunow[33] who gives $A = 4{\cdot}07$; $B = 5{\cdot}93$.

These results were all obtained on the basis of direct measurements of surface shear force on a floating element of finite spanwise extent which averages out the short wavelength quasi-periodic transverse variations that may be expected in any real turbulent layer (*see* Head and Rechenberg[14], whereas the velocity profile will only have been measured for a single spanwise station and will not necessarily be appropriate to the average value of c_f that is obtained.

Now, whilst any such discrepancies may average out over several different experimental arrangements, the possibility cannot be ruled out that the presence of localised three-dimensional effects near the wall leads to a real variation in the values of A and B.

However, for the present purposes the chosen combination of A and B values represents an acceptable averaging of the boundary-layer results and lies close to the most reliable values, obtained from pipe data, where the skin-friction appears to have been accurately determined.

3.3. *The Correlation for γ_s.*

The form of the semi-logarithmic (Clauser) plot of $\dfrac{u}{U_1}$ *vs.* $\log_{10}\dfrac{U_1 y}{\nu}$, corresponding to his particular choice of inner law profile, was prepared and used by Sarnecki to examine many mean velocity profiles from the experiments of Newman[21], Clauser[2] and Ludwieg and Tillmann[20]. The appropriate member of the family of curves on the Clauser plot was fitted to the inner portion of each measured profile in turn, and the function γ_s was determined from the difference between the extrapolated inner profile and the measured velocity distribution, using equation (6) in the form,

$$\gamma_s = \frac{u - U_1}{u_t - U_1}. \tag{10}$$

The final form of the correlation for γ_s is shown in Fig. 5, and included the results of an examination of his profiles measured in zero pressure-gradient boundary layers developing under the action of continuously distributed suction. In the latter case, the inner law and hence the turbulent-fluid velocity distribution was of the bilogarithmic form as given by Black and Sarnecki[1].

As Fig. 5 shows, γ_s appears to be very closely a universal function for layers developing on smooth walls and with small free-stream turbulence levels, independent of the previous history of the flow or of such local parameters as H, R_θ and Γ_1.

That is,

$$\gamma_s = \gamma_s\left(\frac{y}{\delta_s}\right), \text{ only,} \tag{11}$$

where δ_s has been chosen as a convenient definition of the boundary-layer thickness and is equal to twice the height from the surface for which $\gamma_s = 0{\cdot}5$. In these co-ordinates, γ_s is nearly anti-symmetrical about $(0{\cdot}5; 0{\cdot}5)$ and is taken to be zero at $\dfrac{y}{\delta_s} = 1{\cdot}0$, whilst $\gamma_s = 1{\cdot}0$, for $0 \leqslant \dfrac{y}{\delta_s} \leqslant 0{\cdot}075$†. It should be noticed that no adjustment to δ_s can produce agreement between the measured intermittency (γ_k) and this empirical function γ_s, but whether or not the physical basis for Sarnecki's model is accepted as being sound in view of this disagreement, there can be no doubt that it is a very convenient method of building up profiles and has at least as much physical significance as any alternative approach.

†The form of γ_s used in calculations is given as Table 1.

3.4. *The Preparation and Presentation of the Profile Charts.*

The profiles were constructed from numerical solutions of equation (6), using the two universal functions shown in Figs. 4 and 5.

Thirty-six profiles were evaluated, each corresponding to a particular combination of the parameters c_f and $R_{\delta s} = \dfrac{U_1 \delta_s}{\nu}$. That is, the profile family was obtained initially in the form,

$$\frac{u}{U_1} = f\left(\frac{y}{\delta_s}, c_f, R_{\delta s}\right). \tag{12}$$

The values of H and R_θ were found by means of graphical integrations and, after suitable cross-plotting, the final presentation was obtained in the form of charts showing $\dfrac{y}{\theta}$ contours for constant $\dfrac{u}{U_1}$ in the H, R_θ plane.

That is, the new family has the final form,

$$\frac{u}{U_1} = f\left(\frac{y}{\theta}, H, R_\theta\right), \tag{13}$$

and the charts are shown as Figs. 6a to 6n inclusive, for the values:

$$\frac{u}{U_1} = 0{\cdot}10,\ 0{\cdot}20,\ 0{\cdot}30,\ 0{\cdot}40,\ 0{\cdot}50,\ 0{\cdot}60,\ 0{\cdot}70,\ 0{\cdot}80,\ 0{\cdot}90,\ 0{\cdot}95,\ 0{\cdot}98,\ 0{\cdot}99,\ 0{\cdot}995,\ 1{\cdot}00.$$

This presentation is convenient to use, covers a wide range of Reynolds numbers ($10^{2{\cdot}5} \leqslant R_\theta \leqslant 10^{5{\cdot}5}$) in a compact fashion, and requires no interpolation between charts when used to construct a profile. The lower limit of $R_\theta = 320$ corresponds to a criterion given by Preston[23] for the minimum Reynolds number for fully turbulent profiles.

For a given value of c_f, the maximum Reynolds number for which the calculated profiles are acceptable on physical grounds is found from the condition that

$$u = U_1; \frac{du}{dy} = 0, \text{ for all } y \geqslant \delta_s, \tag{14}$$

and

$$u \leqslant U_1; \frac{du}{dy} \geqslant 0, \text{ for all } y < \delta_s. \tag{15}$$

Now, the condition (14) is automatically satisfied provided that $\gamma_s = 0; \dfrac{d\gamma_s}{dy/\delta_s} = 0$ for all $y \geqslant \delta_s$, and this is true for the mean curve used here.

From equation (10) it can be seen that, since $\gamma_s > 0$ for $y < \delta_s$, then, provided $u_t \leqslant U_1$ everywhere in the layer, $u \leqslant U_1$ as required by (15). Furthermore, it can be shown that u_t and u both grow monotonically with y under these conditions, and hence that real profiles will be predicted as long as $u_t \leqslant U_1$ at $y = \delta_s$. The limiting condition therefore becomes,

$$u_t = U_1 \text{ at } y = \delta_s. \tag{16}$$

From equations (4) and (16) we have

$$U_1 = U_\tau \left(5{\cdot}4 + 5{\cdot}5 \log_{10} \frac{U_\tau \delta_s}{\nu} \right),$$

and this gives the expression from which the upper limit to the Reynolds number can be calculated:

$$\log_{10}\left(R_{\delta s\,\max}\right) = \frac{1}{5{\cdot}5}\sqrt{\frac{2}{c_f}} - \frac{5{\cdot}4}{5{\cdot}5} + \log_{10}\sqrt{\frac{2}{c_f}}. \tag{17}$$

As this limit (shown in Fig. 23) is approached, the predicted profiles will be expected to show an unnaturally slow approach to the free-stream velocity. The value δ_s will thus be an over-estimate of the boundary-layer thickness.

The charts for $\frac{u}{U_1} = 0{\cdot}99$, $0{\cdot}995$ and $1{\cdot}00$ were therefore revised on the following basis:

For all fully turbulent conditions the velocity defect in the extreme outer part of the boundary layer adjoining the free stream, should depend only on the distance from the edge of the layer and on the local fluid properties with the exception of viscosity.

That is,

$$f(U_1 - u,\ \delta - y,\ L^*,\ U^*,\ \rho) = 0, \tag{18}$$

where L^*, U^* are the length and velocity scales, respectively, of the flow in this region.

In non-dimensional terms, equation (18) becomes

$$\frac{1 - \left(\frac{y}{\delta}\right)_{\frac{u}{U_1}}}{L^*/_\delta} = f\left[\frac{1 - \frac{u}{U_1}}{U^*/U_1}\right]. \tag{19}$$

Hence, assuming that this region extends towards the surface at least as far as the height for which $\frac{u}{U_1} = 0{\cdot}95$, then choosing this latter point as the reference we may put

$$\frac{U^*}{U_1} = 0{\cdot}05\,; \quad \frac{L^*}{\delta} = 1 - \left(\frac{y}{\delta}\right)_{\frac{u}{U_1} = 0{\cdot}95}. \tag{20}$$

That is,

$$\frac{1 - \left(\frac{y}{\delta}\right)_{\frac{u}{U_1} = k}}{1 - \left(\frac{y}{\delta}\right)_{\frac{u}{U_1} = 0{\cdot}95}} = f\left(1 - \frac{u}{U_1}\right) = f(1-k). \tag{21}$$

Now, the profiles already calculated from the unmodified Sarnecki approach were assumed to be physically acceptable in this outer region provided $H \geqslant 2{\cdot}0$, and so the required relationship (21) was found from the mean curve through these outer profiles. This mean curve is shown in Fig. 7 together with the envelope of the results obtained from the original theory.

Finally, the initial charts were presumed to be correct for $\frac{u}{U_1} \leqslant 0{\cdot}98$ and provided the limit specified by equation (17) was not exceeded, then the revised values of $\frac{y}{\theta}$ for $\frac{u}{U_1} = 1{\cdot}00$, 0·995 and 0·99 could be calculated and these are shown in Figs. 6a to c respectively. The use of this more plausible outer profile then allowed the charts to be extrapolated (on suitable cross-plots) slightly beyond the original limiting curve although it should be remembered that the occurrence of low values of H is generally associated, in practice, with strong favourable pressure gradients where the usual form of the inner law cannot be expected to hold (Launder[19]).

The revised definition of boundary-layer thickness is called δ_1.

In spite of the care taken during the graphical procedure used to construct the charts some slight scatter may be found when profiles are plotted out. However, provided all the charts are used there is very little uncertainty in drawing the mean curve through the points, even for small values of H and R_θ, and the small discrepancies are considered to be quite unimportant.

3.5. *Comparisons with Measured Velocity Profiles.*

Comparisons with measured profiles taken from thirteen experimental boundary layers covering a wide range of conditions, are presented in Figs. 8 to 22, in the natural co-ordinates $\frac{u}{U_1}$ *vs.* $\frac{y}{\theta}$.

The excellent agreement in the majority of cases shown was only achieved, however, after all the measured profile data presented by the original authors had been replotted, smoothed and integrated afresh to obtain the values of H and R_θ given on the figures. These new values were often significantly different from the published values and Fig. 8 shows two important examples taken from the data of Schubauer and Klebanoff[31]. It is seen that better agreement results from the use of the recalculated values, particularly as regards H. The presentation in terms of $\frac{y}{\theta}$ is very useful as it reveals differences in H by the difference in the area between the profiles and the lines $y = 0$; $\frac{u}{U_1} = 1{\cdot}0$, since

$$\int_0^\infty \left(1 - \frac{u}{U_1}\right) d\,\frac{y}{\theta} = \frac{\delta^*}{\theta} = H\,. \tag{22}$$

The greatest inaccuracy to be expected from plotting points, choosing a mean curve, and the actual integration, may be estimated from experience as approximately $\pm$ 2 per cent in H, and although no such estimate can be rigorously justified, the results of the present investigation are self-consistent to a much larger degree than the results shown by different authors in the literature, where errors of up to $\pm$ 7 per cent in H can be found. Overestimates of 20 per cent in R_θ for two of von Doenhoff and Tetervin's profiles were discovered† and are particularly surprising, and whilst not repeated elsewhere, nevertheless meant that *all* such data had to be completely checked.

Agreement with the profiles of *Smith and Walker*[34] is very good, as shown in Fig. 9. The extreme outer parts of the profile are predicted accurately and justify the modified definition of boundary-layer thickness (δ_1) used in the charts. For the equilibrium layers of *Clauser*[2], Figs. 10 and 11 show an excellent overall agreement, marred only by the small systematic discrepancies near to the wall in Clauser I.

The aerofoil measurements of *Newman*[21] are shown in Fig. 12 where the profiles at stations F and G, just before separation, show small systematic inaccuracies which may be traced to the choice of best-fit mean lines on the Clauser plot used by Sarnecki when making his correlation for γ_s.

The more recent measurements of *Schubauer and Spangenberg*[32] were not available to Coles or to Sarnecki when they were preparing their correlations but are incorporated here and provide an inde-

†*See* Fig. 8 of Thompson[40].

pendent test of the new profile family. Figs. 13, 14 and 15 reveal quite satisfactory agreement, although the shape of the separation profile of layer 'C', at $x = 200$ in., is not accurately known near to the wall.

Fig. 16 shows some typical profiles, in the region of falling pressure of the boundary layer of *Schubauer and Klebanoff*[31]. Agreement with experiment is good in both the inner and outer regions. In the adverse pressure gradient portion of the same layer, the level of agreement is quite satisfactory, as seen in Fig. 17, except for the details of the inner profile, where, as may be expected, systematic departures from the logarithmic behaviour become more pronounced as separation is approached although the experimental points for $x = 25{\cdot}4$ ft, and $25{\cdot}77$ ft are rather scattered and make interpretation of any overall trends rather difficult.

The data of *von Doenhoff and Tetervin*[8] provides a poorer test of the new profile family, as each measured profile is defined by only a few comparatively scattered points. However, the calculated profiles, as shown in Figs. 18 and 19 provide entirely plausible mean lines through these measured values. Predictions for the inner profiles and the approach to the free stream conditions appear to be quite satisfactory. The extensive viscous region near the wall, characteristic of low overall Reynolds numbers, is demonstrated especially clearly in Fig. 18. The discrepancy between these profiles and those measured by Clauser, for the same H values, is adequately accounted for by the new profile family which allows for the very different Reynolds numbers in the two cases. An interesting feature is the quite good agreement obtained at $\frac{x}{c} = 0{\cdot}075$, which is only of the order of ten boundary-layer thicknesses downstream of the transition device which consisted of surface roughness extending back to $\frac{x}{c} = 0{\cdot}050$. In spite of the falling H value in this region of adverse pressure gradient, it appears that transition may be regarded as complete, as the profiles follow the behaviour of a model which contains no explicit reference to transition conditions.

Schmidbauer[29] showed only the profiles at the beginning of his boundary layer on a convex surface. In spite of the low Reynolds number, it is apparent that the layer may be considered to be fully turbulent for $x \geqslant 46$ *cm*, where good agreement between the predicitions of the new family and the measured profiles is obtained, as shown in Fig. 20.

Fig. 21 shows the streamwise velocity profiles obtained from the measurements of *Kuethe, McKee Curry*[18], in the strongly three-dimensional layer developing on a swept wing of elliptic planform at an incidence just below the stall. Considering the nature of the experimental conditions and the difficulties encountered when reducing the data from the original presentation, the level of agreement is very encouraging and suggests that this profile family may be suitable for streamwise velocity distributions in three-dimensional flows, although the detailed assumptions for the inner region are unlikely to be satisfactory and hence a revised skin-friction law may be needed.

Finally, a comparison with the profiles measured by *Stratford*[37] on a concave wall with an initially severe adverse pressure gradient, is presented in Fig. 22. The two-parameter family gives poor agreement with experiment at the beginning of the layer, where $C_p = 0{\cdot}122$ and $0{\cdot}200$. The measured profiles are similar in shape to those that would be predicted by the profile family at rather smaller Reynolds numbers.

3.6. *The New Skin-friction Law.*

The use of the inner law profile shown in Fig. 4 allows the skin friction to be related to the overall profile parameters H and R_θ. Fig. 23 shows the new relationship, with contours of c_f chosen so that linear interpolation leads to an error which is much less than the uncertainties present in the underlying theory. The limiting curve corresponding to equation (17) is shown in the figure.

Comparison with the earlier law of Ludwieg and Tillmann[20] may be made using Fig. 24.

The newer law should predict better skin-friction values near to separation as zero skin friction is predicted at a limiting H value of $4{\cdot}24$, whereas according to Ludwieg and Tillmann's relationship this does not occur unless H takes an infinite value.

The earlier law was supported by measured data only in the range $1{\cdot}2 \leqslant H \leqslant 2{\cdot}0$; $1000 \leqslant R_\theta \leqslant 20000$, and was based on the particular numerical values of the inner law constants A, B, that were obtained in Ludwieg and Tillmann's own experiments. That is, they used the logarithmic law

$$\frac{u}{U_\tau} = 6{\cdot}0 + 5{\cdot}2 \log_{10} \frac{U_\tau y}{\nu}. \tag{23}$$

The different assumptions for the values of the constants A and B in the two laws (4) and (23) result in larger values of c_f being predicted by Ludwieg and Tillmann's relationship in the range of Reynolds numbers $2000 \leqslant R_\theta \leqslant 50\,000$, approximately. At lower Reynolds numbers, the larger values predicted by the newer law must be due to the difference in the outer region assumptions used in the two cases.

3.7. *Shape-factor Relationships.*

Values of energy loss thickness ε, where

$$\varepsilon = \int_0^\infty \frac{u}{U_1} \left[1 - \left(\frac{u}{U_1}\right)^2\right] dy,$$

and hence of $H_\varepsilon \left(= \frac{\varepsilon}{\theta}\right)$ have been calculated for the new profile family. The dependence of H_ε on H and R_θ is shown in Fig. 25 where it is compared with the single curve derived from power law profiles of the form

$$\frac{u}{U_1} = \left(\frac{y}{\delta}\right)^{\frac{1}{n}}$$

as used by Rubert and Persh[27] and Walz[45] in their calculation methods which employed the energy integral equation as the auxiliary equation. Further comparisons with earlier relationships may be made by reference to the paper by Fernholz[11].

Head[13] assumed a singly infinite relationship between the parameter $H_{\delta-\delta^*} \left(= \frac{\delta-\delta^*}{\theta}\right.$ where $\delta = y, \frac{u}{U_1} = 0{\cdot}995\left.\right)$ and H, from a consideration of the measured profiles of Newman[21] and Schubauer and Klebanoff[31]. Head's curve is compared with the predictions of the new family in Fig. 26 where it can be seen that his relationship is reasonable for $R_\theta > 5 \times 10^3$ but is rather less satisfactory at smaller Reynolds numbers.

The new relationships shown in Figs. 25 and 26 are suitable for direct use in shape-factor calculations if the interpolation with respect to R_θ is made carefully.

4. *Discussion.*

4.1. *The Comparisons with Measured Profiles.*

The profile data used in this investigation have not been corrected for instrument errors due to turbulence or mean velocity gradient. This assumes that, if these corrections are not negligible then they are almost uniquely defined by the profile parameters H and R_θ, and consequently the possible variations between uncorrected velocity profiles for given H and R_θ values should be much smaller than any systematic inaccuracies due to defects in the profile model itself.

In most cases, the velocity profiles have been obtained from pitot traverses and single measurements of static pressure at the wall. The effect of static pressure variation due to streamline curvature imposed by curvature of the wall, has been estimated from the following equations:

$$\frac{\partial p}{\partial y} = \frac{\rho u^2}{R}\,;\, \frac{1}{2}\rho u^2 = p_0 - p(y)\,;\, \frac{1}{2}\rho U_1{}^2 = P_0 - p(\delta_1).$$

Power law profiles $\frac{u}{U_1} = \left(\frac{y}{\delta_1}\right)^{\frac{1}{n}}$, where $1 \leqslant n \leqslant 10$, corresponding to $3{\cdot}0 \geqslant H \geqslant 1{\cdot}2$, were considered for $\left|\frac{\delta_1}{R}\right| = 0{\cdot}025$, in order to find the maximum errors likely to be encountered in the boundary-layer measurements that have been used to test existing calculation methods (Thompson[40]). It was found that the effect on H and R_θ is very small unless H falls below 1·3 when $\left|\frac{\delta_1}{R}\right| > 0{\cdot}02$.

For the profiles measured on convex walls R_θ is lowered by 3 per cent or less, however for the very severe conditions in Stratford's layer on a concave wall the effect is greater. As shown in Fig. 22, for $C_p = 0{\cdot}200$, where $H = 1{\cdot}8$ and $\left|\frac{\delta_1}{R}\right| = 0{\cdot}035$, H is insignificantly affected but R_θ is raised by 6 per cent. In all cases, however, the use of corrected values of H and R_θ does not seem to alter the level of agreement (or disagreement) between the new profile family and experiment. It appears, therefore, that moderate wall curvature alters the mixing in the layer and hence its development is changed for a given pressure distribution, but the profiles in the new development are for all practical purposes still selected from the same family.

The good agreement obtained with the profiles at very low R_θ values in Figs. 18, 19 and 20, means that any new calculation method based upon this family should not require the rather artificial starting assumptions found in some of the earlier published methods.

An examination of the comparisons with profiles measured in layers developing on flat surfaces shows that the new family represents a quite satisfactory averaging of the inner profiles obtained in several different experiments, but some systematic deviations may be observed in some individual experiments. For example, in Fig. 10 the predicted velocities for $\frac{y}{\delta_1} \leqslant 0{\cdot}15$ approximately, tend to be too low, whilst for the remaining experiments, the predicted velocities tend to be in better agreement with experiment or slightly too high.

In conditions of strong adverse pressure gradient and small surface shear, the simple 'universal' inner profile cannot be expected to hold and this leads to the disagreement in the detailed profile shapes already noted for Newman (Fig. 12) and for Schubauer and Klebanoff (Fig. 17).

If a slightly different 'intermittency' distribution had been used, rising to $\gamma_s = 1{\cdot}0$ at $y = 0$, instead of at $y \approx 0{\cdot}1\ \delta_s$, then improved agreement would have been obtained in these conditions. Coles' choice of 'wake law' does in fact provide a fortuitous allowance for the effects of the adverse pressure gradient in these two layers as it does not take a zero value throughout the inner region.

The present family will be more accurate than Coles' in conditions of small pressure gradient but if it is desired to calculate shear stresses from the boundary-layer equations using a profile family, some direct account of the influence of pressure gradient on the inner profile may be needed.

4.2. *The effect of adverse pressure gradient on the 'universal' features of the profile model.*

The work of Townsend[43,44], Szablewski[38] and others has shown that the form of the inner region profile must change from the constant stress law,

$$\frac{u}{U_\tau} = f\left(\frac{U_\tau y}{\nu}\right), \tag{24}$$

to the limiting form for zero stress (but not necessarily zero pressure gradient),

$$\frac{u}{\left(\frac{\nu}{\rho}\frac{dp}{dx}\right)^{1/3}} = g\left(\frac{y^3}{\nu^2}\frac{1}{\rho}\frac{dp}{dx}\right), \tag{25}$$

as the stress variation $\frac{\tau(y)}{\tau_0}$ through the inner region becomes larger.

In general, dimensional analysis suggests an inner profile of the form,

$$\frac{u}{U_\tau} = f\left(\frac{U_\tau y}{\nu}, \frac{\tau}{\tau_0}, \frac{y}{\delta}\right), \tag{26}$$

Now, if the shear stress distribution *not too far from the wall* is satisfactorily specified by the addition of a second boundary condition

$$\left(\frac{\partial \tau}{\partial y}\right)_0 = \frac{dp}{dx}, \tag{27}$$

then

$$\frac{\tau}{\tau_0} = 1 + \frac{y}{\tau_0}\frac{dp}{dx},$$

$$= 1 + \frac{U_\tau y}{\nu} \cdot \frac{\nu}{U_\tau^3}\frac{1}{\rho}\frac{dp}{dx}. \tag{28}$$

Hence (26) becomes

$$\frac{u}{U_\tau} = f\left(\frac{U_\tau y}{\nu}, \frac{\nu}{U_\tau^3}\frac{1}{\rho}\frac{dp}{dx}\right). \tag{29}$$

Sufficiently close to the wall, the constant stress approximation will be accurate, but, the effects of the pressure gradient will produce a cumulative departure from the simple form (24) which will be distinguished experimentally beyond a value of $\frac{U_\tau y}{\nu}$ which will depend upon the value of the parameter $\frac{\nu}{U_\tau^3}\frac{1}{\rho}\frac{dp}{dx}$ which will now be referred to as Δ.

The use of the conventional 'universal' form equation (24) in adverse pressure gradients has always been supported by the appearance of many profiles which can be matched by a member of the family of curves on a Clauser plot, and, more directly, by the skin-friction measurements of Ludwieg and Tillmann[20], where no additional uncertainty concerning the values of A and B in the logarithmic law was found when compared with the results for pipes, channels and zero-pressure gradient boundary layers.

However, as shown recently by Rotta[26], even the 'very strong adverse pressure gradient' conditions of Ludwieg and Tillmann corresponded only to values of $\Delta \leqslant 0{\cdot}005$, and under these conditions measurable deviations from the universal inner law do not occur if $\frac{U_\tau y}{\nu} \leqslant 400$, approximately, with an even larger range of $\frac{U_\tau y}{\nu}$ being observed as the constant pressure conditions are approached (provided that in all cases $\frac{y}{\delta} \leqslant 0{\cdot}1$, approximately, so that the outer part of the layer has little effect).

In some of the profiles of Stratford, Schubauer and Klebanoff, and Newman, as mentioned earlier, the range of the 'universal' inner profile is very much less and no logarithmic portion can be found, as shown in Fig. 27. From this figure and a re-examination of Sarnecki's original correlation for Newman's profiles, it is seen that a universal form for γ_s can be obtained only by a rather drastic approximation to the inner profile as shown by the solid lines corresponding to the skin-friction values given by the new law (Fig. 23). Under these conditions the existing two-parameter laws will over-estimate the skin friction

by an increasing amount as Δ becomes larger†, also it appears that the simple outer region functions representing the departure of the overall velocity distribution from the inner region profile are no longer universal, as, replacing the expression (4) for u_t by an inner profile similar to that suggested by Szablewski[38] from the use of mixing length theory and the assumption of a linear stress variation. $\left(\tau = \tau_0 + y\frac{dp}{dx}\right)$, did not recover the normal form for γ_s once non-universality had penetrated as far as the blending region, and it is to be expected that the 'Wake law' is similarly affected.

It is suggested, therefore, that the simple two-parameter representation will become progressively less accurate when the deviation from the simple inner law, equation (24), is apparent at $\frac{U_\tau y}{\nu} = 100$. This is equivalent to $0{\cdot}1 > \Delta > 0{\cdot}01$, approximately, as shown from Fig. 28, and discussed below.

The maximum range of $\frac{U_\tau y}{\nu}$ for which equation (24) is accurate can be found (approximately) as a function of Δ from the examination of the above mean velocity profiles with the use of a linear stress profile to suggest an improved value of c_f and hence the point of departure, on the Clauser plot, from the simple inner profile form. This relationship is plotted in Fig. 28, and is confirmed by the direct measurements of Head and Rechenberg[14] where, in the pressure rise before a step, their disagreement between the skin friction readings obtained from a small sublayer fence and a larger Preston tube can be used to determine the maximum extent of $\frac{U_\tau y}{\nu}$ over which the simple universal behaviour, equation (24), (and hence their calibration) remains true.

Fig. 28 can be used to assist in the analysis of velocity-profile data in the future, although the construction of a Clauser plot with families of linear stress law curves for various values of Δ, for each c_f value, would be a further improvement, but this may not yet be possible due to uncertainties over the coefficients in these laws, also the actual stress variations of the profiles considered will lie between the constant stress and linear stress distributions due to the effect of the actual rate of development of the mean flow $\left(\text{that is, to } u\frac{\partial u}{\partial x} + v\frac{\partial u}{\partial y}\right)$, and so the real inner profile may be expected to be intermediate in behaviour between a linear stress and a logarithmic profile.†

4.3. *The Requirements for the Accuracy of the Skin friction Law and of Profile Shape in Boundary-layer Calculations.*

The values of A and B in the logarithmic law, equation (4), have been regarded as representing the averages of the values obtained from those experiments in which skin friction has been directly measured, with some weighting towards the more reliable estimates obtained in fully developed pipe flow. The new skin-friction law should therefore predict the average of the values that might be measured for a given combination of H and R_θ, if $\Delta \leqslant 0{\cdot}01$ approximately, with a maximum uncertainty of ± 20 per cent if the spread of the values of A and B, mentioned in Section 3.2. is due to a real physical non-similarity.

This represents a maximum error of ± 20 per cent in calculated $\frac{dR_\theta}{dx}$ in zero pressure gradients, becoming rather smaller in most rising pressure layers. This is of importance when interpreting the momentum calculations described in Section 3.2. of Thompson[40] and shows that the discrepancies between the simple two-dimensional theory and experiment cannot usually be explained by errors in the new skin-friction law, except very near to separation.

---

†Using a linear stress analysis as mentioned later, improved values of c_f can be obtained and it is thought that at $\Delta = 0{\cdot}03$ approximately, c_f is in error by $+25$ per cent, whilst if $\Delta > 0{\cdot}1$, c_f is in error by $+60$ per cent or more.

†Recent work by Patel[22] has resulted in a more accurate assessment of the effects of pressure gradient on the inner profile.

In conditions where $\Delta > 0{\cdot}01$, the use of the ordinary inner profile form, equation (24), introduces an additional systematic over-estimation of skin friction. It is possible that this might have a significant effect on the calculation of momentum thickness in these conditions. To investigate this, calculations of momentum-thickness development have been made for Stratford's layer using the two-dimensional momentum integral equation,

$$\frac{dR_\theta}{dx} = \frac{c_f}{2}\frac{U_1}{\nu} - (H+1)\frac{R_\theta}{U_1}\frac{dU_1}{dx} \tag{30}$$

and measured H values, together with two alternative assumptions for skin friction, namely that $c_f = c_f(H, R_\theta)$ from the new law shown in Fig. 23 or alternatively that there is zero skin friction throughout the entire layer. The results of these calculations are presented in Fig. 29 and show that the maximum possible overestimation of c_f due to the use of the new law, only produces an increase of 5 per cent in the calculated slope $\frac{dR_\theta}{dx}$.

The disagreement between the result for zero skin friction and the experimental momentum growth was attributed, by Stratford, to three-dimensional flow, although neither the values of H and R_θ nor the form of the momentum equation (30) have been corrected for the static-pressure variations normal to the wall and this makes the interpretation of this disagreement more difficult.

If Δ is much larger than the value 0·01, the disagreement between the measured profiles and the two-parameter family is of the same order as that previously noted between experiment and one-parameter profiles, for smaller values of this pressure gradient parameter. This suggests that if a prolonged development under such conditions is possible then it is unlikely to be satisfactorily calculated by any method, developed for less severe conditions, which involves profile assumptions that take no account of the direct effects of stress variations near the wall. This can only be ascertained on the basis of direct shape-factor calculations, however, and it is possible that such considerations will only become important in the conditions of strongly rising pressure that might be encountered by sucked turbulent layers.

5. *Conclusions.*

(i) The use of an explicit presentation has enabled the new profile family to be compared directly with a wide range of measured profiles, and a very satisfactory level of agreement is obtained in most cases.

(ii) The disagreement between the profiles of Clauser and of von Doenhoff and Tetervin having the same H values has been shown to be due to the different Reynolds numbers in the two cases.

(iii) Agreement between the new profile family and measured profiles can be used to define the extent of 'fully turbulent' flow and hence the most upstream starting position for a turbulent boundary-layer calculation can be found.

(iv) The addition of a third parameter $\left(\Gamma_1 = \frac{-\theta}{U_1}\frac{dU_1}{dx}, \text{ say}\right)$, to allow for the effects of shear stress variations on the inner region velocity distribution and hence on the 'universal' features of the profile model, will only become necessary if the pressure gradient parameter $\frac{\nu}{U_\tau^3}\frac{1}{\rho}\frac{dp}{dx}$ takes a value greater than about 0·01.

If a *prolonged* development under such conditions *is* possible, on solid surfaces, then the use of the existing skin friction and shape-factor relationships may lead to appreciable errors, but for all the layers used as a basis for the comparisons of H and R_θ calculations presented in a previous report (Thompson[40]) the new skin friction law appears to be entirely satisfactory.

(v) Further investigation into the effect of pressure gradient and of both gross and localised three-dimensional phenomena on the wall region properties is clearly needed.

Finally, it should be noticed that the present approach is readily adaptable in principle to account for the effects of wall roughness, or of distributed suction or injection, for example, by substituting the

appropriate inner region velocity profile for the present choice of turbulent fluid velocity distribution.

An investigation of the effects of distributed suction on profile shape and on boundary layer development is being conducted by the author and it is hoped to publish full details of this work in a future report.

6. *Acknowledgements.*

The author gratefully acknowledges the guidance and advice he received from Dr. M. R. Head who supervised this work whilst the author was a research student at Cambridge University. Thanks are also due to Miss Susan Gray for her assistance with the numerical work and to the staff of the Drawing Office for their care in tracing the profile charts.

NOTATION

A, B constants in the semi-logarithmic inner law $\left(B = \frac{1}{\kappa} \log_e 10\right)$

c aerofoil chord length

c_f local value of skin friction coefficient $\left(= \frac{\tau_0}{\frac{1}{2}\rho U_1^2}\right)$

C_p pressure coefficient defined by Stratford $\left(= 1 - \frac{U_1^2}{U_0^2}\right)$

$H, H_{\delta-\delta^*}, H_{\varepsilon},$ profile shape-factors: $H = \frac{\delta^*}{\theta}$; $H_{\delta-\delta^*} = \frac{\delta - \delta^*}{\theta}$; $H_\varepsilon = \overline{H} = \frac{\varepsilon}{\theta}$.

M, N coefficients appearing in the semi-logarithmic inner law when written in co-ordinates $\frac{u}{U_1}$ *vs.* $\log_{10} \frac{U_1 y}{\nu}$ (used in Section 3.2. (ii))

p local static pressure at (x, y)

p_0 local total pressure at (x,y)

P_0 local total pressure in the free-stream ($P_0 = p(\delta_1) + \frac{1}{2}\rho U_1^2$) where $p(\delta_1)$ is the local static pressure at $(x, y = \delta_1)$

R local radius of curvature of surface (in the $x-y$ plane)

$R_x, R_\theta, R_c, R_{\delta_s}$ Reynolds numbers: $R_x = \frac{U_1 x}{\nu}$; $R_\theta = \frac{U_1 \theta}{\nu}$; $R_c = \frac{U_1 c}{\nu}$; $R_{\delta_s} = \frac{U_1 \delta_s}{\nu}$

$(R_{\delta_s})_{\max}$ limiting value of R_{δ_s}

U_1 component of free-stream velocity vector along the x-direction

u x-component of the velocity vector in the boundary layer

U_0 value of U_1, at the reference station $x = x_0$

U_τ local value of wall shear velocity $= \sqrt{\frac{\tau_0}{\rho}}$

u_t mean velocity of the turbulent fluid over 'time turbulent'

$\frac{U_1}{\nu}$ local free-stream Reynolds number per unit length

x, y, z localised rectangular Cartesian coordinates: x is measured along the surface in the longitudinal direction; y is the distance from the surface measured along the local normal direction; z is the spanwise distance

$\gamma, \gamma_K, \gamma_s$ intermittency factors (defined in the text)

Γ_1 pressure gradient parameter $\left(= -\frac{\theta}{U_1} \frac{dU_1}{dx}\right)$

$\delta, \delta_1, \delta_K, \delta_s$ various definitions of boundary-layer thickness, that is the value of y for which $\frac{u}{U_1} = 1{\cdot}00$, unless stated otherwise in the text.

NOTATION—*continued*

δ^*	displacement thickness $\left[= \int_0^\infty \left(1 - \frac{u}{U_1}\right) dy\right]$
Δ	inner region pressure-gradient parameter $\left(= \frac{\nu}{U_\tau^3} \frac{1}{\rho} \frac{dp}{dx}\right)$
ε	energy-loss thickness $= \int_0^\infty \left[1 - \left(\frac{u}{U_1}\right)^2\right] \frac{u}{U_1} dy$
η	profile shape factor (used principally by Gruschwitz) $= \left[1 - \left(\frac{u}{U_1}\right)^2\right]_{y = \theta}$
θ	momentum-loss thickness $= \int_0^\infty \left(1 - \frac{u}{U_1}\right) \frac{u}{U_1} dy$
κ	universal constant of proportionality in the mixing length relationship ($l = \kappa y$) used in the wall region
μ	coefficient of viscosity
ν	kinematic viscosity $\left(= \frac{\mu}{\rho}\right)$
ρ	density of fluid
τ	shear stress $\left(= \mu \frac{\partial u}{\partial y} - \rho \overline{u'v'}\right)$
τ_0	wall shear stress
$\lvert\ \rvert$	modulus (absolute value of)

REFERENCES

No.	*Author(s)*	*Title, etc.*
1	T. J. Black and A. J. Sarnecki	The turbulent boundary layer with suction or injection. A.R.C. R. and M. 3387. October, 1965.
2	F. H. Clauser	Turbulent boundary layers in adverse pressure gradients. *J. Aeronaut. Sci.*, Vol. 21, No. 2, pp. 91–108. 1954.
3	F. H. Clauser	The turbulent boundary layer. *Advances in App. Mech.*, pp. 1–51. 1956. Academic Press.
4	D. Coles	The problem of the turbulent boundary layer. *Z.angew. Math. Phys.*, Vol. 5, pp.181–202. 1954.
5	D. Coles	The law of the wake in the turbulent boundary layer. *J. Fluid Mech.*, Vol. 1, pp. 191–226. 1956.
6	S. Corrsin	Investigation of flow in an axially-symmetrical heated jet of air. NACA Wartime Rep. W–94, (previously NACA ACR3L23). 1943.
7	S. Corrsin and A. L. Kistler	The free-stream boundaries of turbulent flows. NACA Report 1244, 1955 (formerly NACA TN 3133).
8	A. E. von Doenhoff and N. Tetervin ..	Determination of general relations for the behaviour of turbulent boundary layers. NACA Report 772. 1943.
9	E. R. van Driest	On turbulent flow near a wall. *J. Aeronaut Sci.*, Vol. 23, pp. 1007–1011 and p. 1036. 1956.
10	R. A. Dutton	The velocity distribution in a turbulent boundary layer on a flat plate. A.R.C. C.P. 453. October, 1957.
11	H. H. Fernholz	A new empirical relationship between the form-parameters H_{32} and H_{12} in boundary layer theory. *J. Roy. Aero. Soc.*, Vol. 66, pp. 588–589. 1962.
12	E. Gruschwitz	The turbulent layer of friction in two-dimensional flow with pressure drop and increase. Translation Ae. Tech. 632, F.M. 79, of Göttingen Dissertation. 1932.
13	M. R. Head	Entrainment in the turbulent boundary layer. A.R.C. R. & M. 3152. September, 1958.
14	M. R. Head and I. Rechenberg	The Preston tube as a means of measuring skin friction. *J. Fluid Mech.*, Vol. 14, Pt. 1; 1962.
15	T. Kawasaki	On an approximate solution of the two-dimensional turbulent boundary layer. Trans. *Japan Soc. Aero. and Space Sci.*, Vol. 4, No. 5, pp. 1–11. 1961.
16	A. Kehl	Investigations on convergent and divergent turbulent boundary layers. R.T.P. Translation No. 2035, from Ing. Archiv., Vol. 13, No. 5, pp. 293–329. 1943.

REFERENCES—*continued*

No.	*Author(s)*	*Title, etc.*
17	P. S. Klebanoff	Characteristics of turbulence in a boundary layer with zero pressure gradient. NACA Report 1247, 1955 (formerly NACA TN 3178, 1954).
18	A. M. Kuethe, P. B. McKee and W. H. Curry ..	Measurements in the boundary layer of a yawed wing. NACA TN 1946. 1949.
19	B. E. Launder	The turbulent boundary layer in a strongly negative pressure gradient. Gas Turbine Laboratory Rep. No. 71–M.I.T. 1963.
20	H. Ludwieg and W. Tillmann	Investigation of the wall-shearing stress in the turbulent boundary layers. NACA TM 1285, 1950. Translated from Ing. Archiv. Vol. 17, pp. 288–299. 1949.
21	B. G. Newman	Some contributions to the study of the turbulent boundary layer near separation. Aust. Dept. Supply Rep. No. ACA–53. 1951.
22	V. C. Patel	Calibration of the Preston tube and limitations on its use in pressure gradients. *J. Fluid Mech.*, Vol. 23, pp. 185–208, September, 1965.
23	J. H. Preston	The minimum Reynolds numbers for turbulent boundary layers and the functions of transition devices. A.R.C. 19,006, January, 1957.
24	D. Ross	A study of incompressible turbulent boundary layers. Ordnance Research Lab. TM ONR Project NR 062–139–1; (Ph.D. Thesis, Harvard University). 1953.
25	D. Ross	A new analysis of Nikuradse's experiments on turbulent flow in smooth pipes. *Proc. Third Midwestern Con. Fluid Mech.* March, 1953.
26	J. C. Rotta	Turbulent Boundary Layers in Incompressible Flow. *Progress in Aeronautical Sciences*, Vol. II, pp. 1–220, Pergamon Press. 1962.
27	K. F. Rubert and J. Persh	A procedure for calculating the development of turbulent boundary layers under the influence of adverse pressure gradients. NACA TN 2478, September, 1951.
28	A. J. Sarnecki	*Ph.D. Dissertation*, Cambridge University. 1959.
29	H. Schmidbauer	Turbulente Reibungsschicht an erhaben gekrümmten Flächen. *Luftfahrtforschung* Vol. 13, pp. 160–162, 1936, (read in a private translation) also NACA TM 791.
30	G. B. Schubauer	Turbulent process as observed in boundary layer and pipe. *J. App. Physics*, Vol. 25, pp. 188–196; also A.R.C. 17,321. 1954.

REFERENCES—*continued*

No.	*Author(s)*	*Title, etc.*
31	G. B. Schubauer and P. S. Klebanoff	Investigation of separation of the turbulent boundary layer. NACA TN 2133 1950; also NACA Report 1030 (1951).
32	G. B. Schubauer and W. G. Spangenberg	Forced mixing in boundary layers. *J. Fluid Mech.*, Vol. 8, pp. 10–32. 1960.
33	G. Schultz–Grunow	Neues Reibungswiderstandsgesetz für glatte Platten. *Luftfahrtforschung*, Vol. 17, pp. 239–246, 1940, translated as NACA TM 986 (1941).
34	D. W. Smith and J. H. Walker	Skin friction measurements in incompressible flow. NACA TN 4231; 1958.
35	D. A. Spence	The development of turbulent boundary layers. *J. Aeronaut Sci.*, Vol. 23, pp. 3–15. 1956.
36	R. W. Stewart	Irrotational motion associated with free turbulent flows. *J. Fluid Mech.*, Vol. 1, pp. 593–606. 1956.
37	B. S. Stratford	An experimental flow with zero skin friction throughout its region of pressure rise. *J. Fluid Mech.*, Vol. 5, pp. 17–35.
38	W. Szablewski	Wandnahe Geschwindigkeitsverteilung turbulenter Grenzschichtströmungen mit Druckanstieg. *Ing. Archiv.*, Vol. 23, pp. 295–306. 1955.
39	B. G. J. Thompson	*Ph.D. Dissertation*, Cambridge University. 1963.
40	B. G. J. Thompson	A critical review of existing methods of calculating the turbulent boundary layer. A.R.C. 26, 109, 1964.
41	A. A. Townsend	Local isotropy in the turbulent wake of a cylinder. *Austr. J. Sci. Res.*, A. Vol. 1, pp. 161–174. 1948.
42	A. A. Townsend	*The Structure of Turbulent Shear Flow.* Cambridge Univ. Press. 1956.
43	A. A. Townsend	The development of turbulent boundary layers with negligible wall stress. *J. Fluid Mech.*, Vol. 8, pp. 143–155. 1960.
44	A. A. Townsend	Equilibrium layers and wall turbulence. *J. Fluid Mech.*, Vol. 11, pp. 97–120. 1961.
45	A. Walz	Beitrag zur Naherungstheorie kompressibler turbulenter Grenzschichten. DVL B. Nr. 84. 1959.

TABLE 1

Values of 'Intermittency' Function $\gamma_s\left(\frac{y}{\delta_s}\right)$

$\frac{y}{\delta_s}$	γ_s	$\frac{y}{\delta_s}$	γ_s	$\frac{y}{\delta_s}$	γ_s
1·0	0·000	0·25	0·869	0·13	0·978
0·95	0·006	0·20	0·923	0·125	0·981
0·90	0·020	0·195	0·928	0·12	0·9835
0·85	0·044	0·19	0·933	0·115	0·986
0·80	0·077	0·185	0·9375	0·11	0·988
0·75	0·127	0·18	0·942	0·105	0·990
0·70	0·190	0·175	0·946	0·10	0·992
0·65	0·263	0·17	0·950	0·095	0·9935
0·60	0·341	0·165	0·954	0·09	0·995
0·55	0·420	0·16	0·958	0·085	0·9965
0·50	0·500	0·155	0·9615	0·08	0·998
0·45	0·580	0·15	0·965	0·075	1·000
0·40	0·659	0·145	0·9685	0·07	1·000
0·35	0·736	0·14	0·972	to	
0·30	0·806	0·135	0·975	0·00	1·000

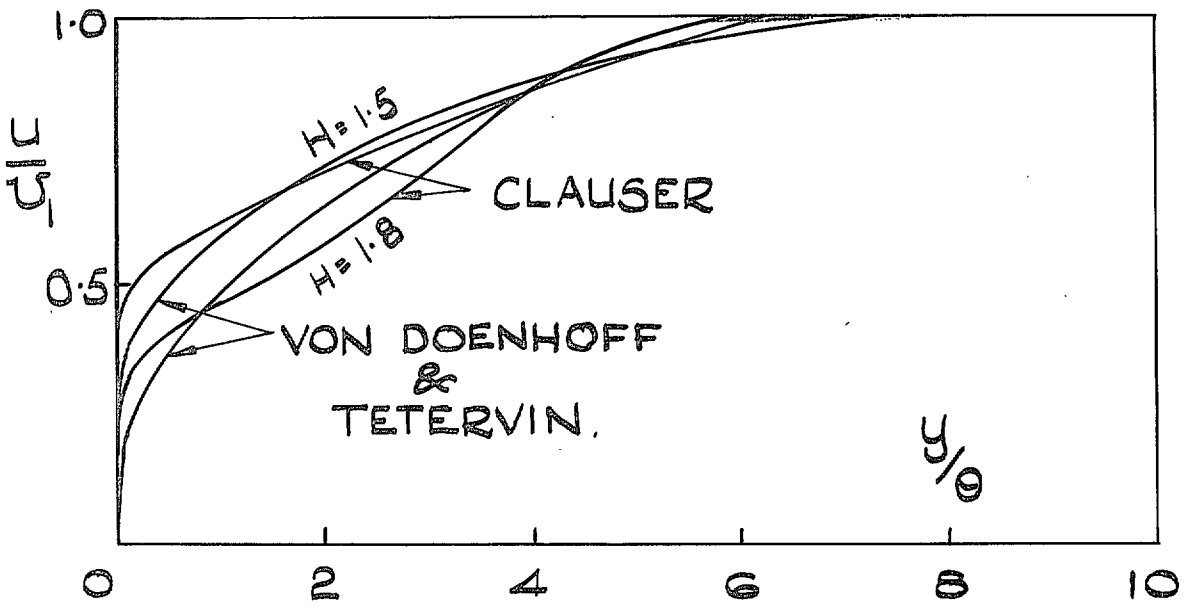

FIG. 1. Comparison of Clauser's measured velocity profiles with the von Doenhoff and Tetervin one-parameter family of profiles [reproduced from Clauser[2]]

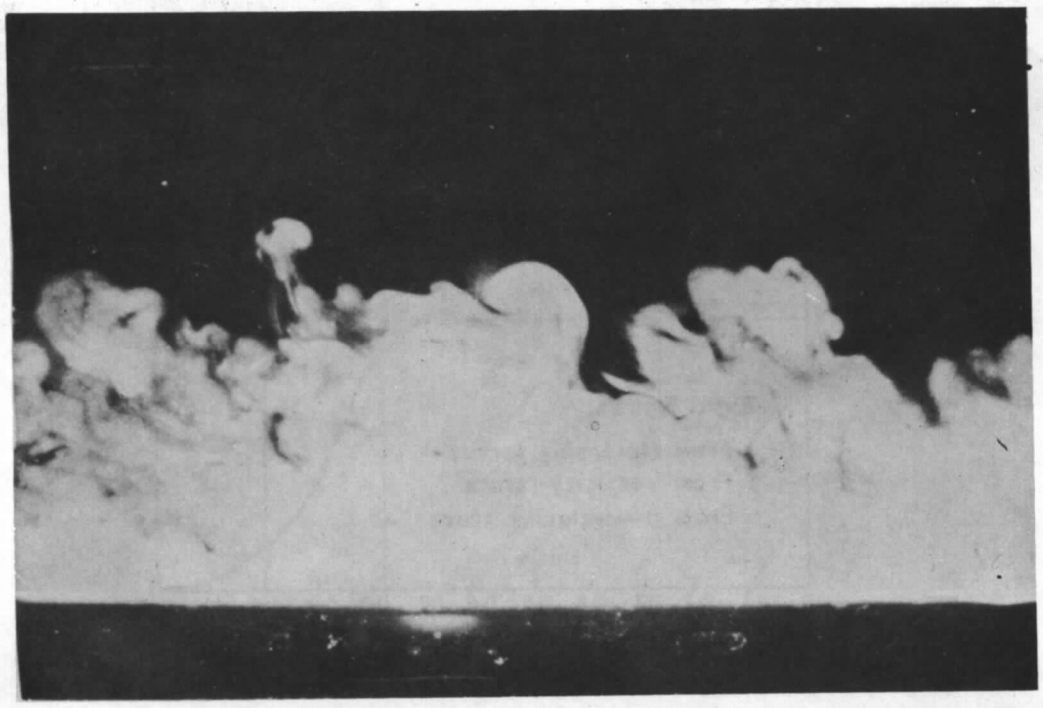

FIG. 2a. $U_1 = 50$ ft/sec., $R_\theta \approx 6000$

FIG. 2b. $U_1 = 10$ ft/sec., $R_\theta \approx 1200$

FIGS 2a and b. Smoke photographs showing intermittency in the zero pressure gradient boundary layer.

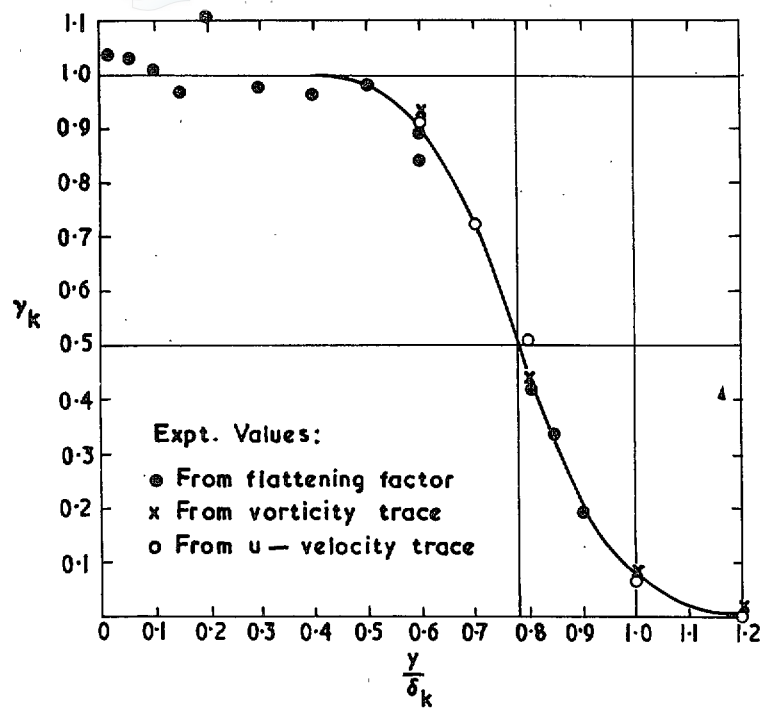

FIG. 3. The distribution of intermittency factor in a zero pressure gradient boundary layer [reproduced from Klebanoff[17]]

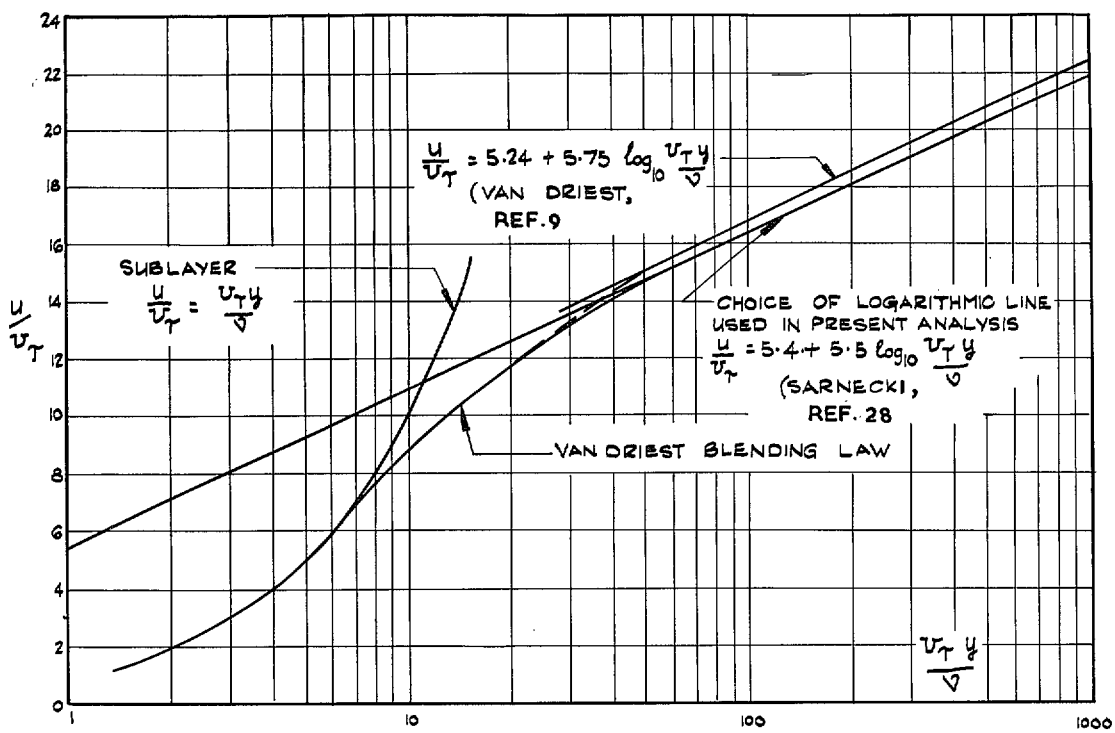

FIG. 4. Wall region velocity variation used for calculating the new mean-velocity profile family.

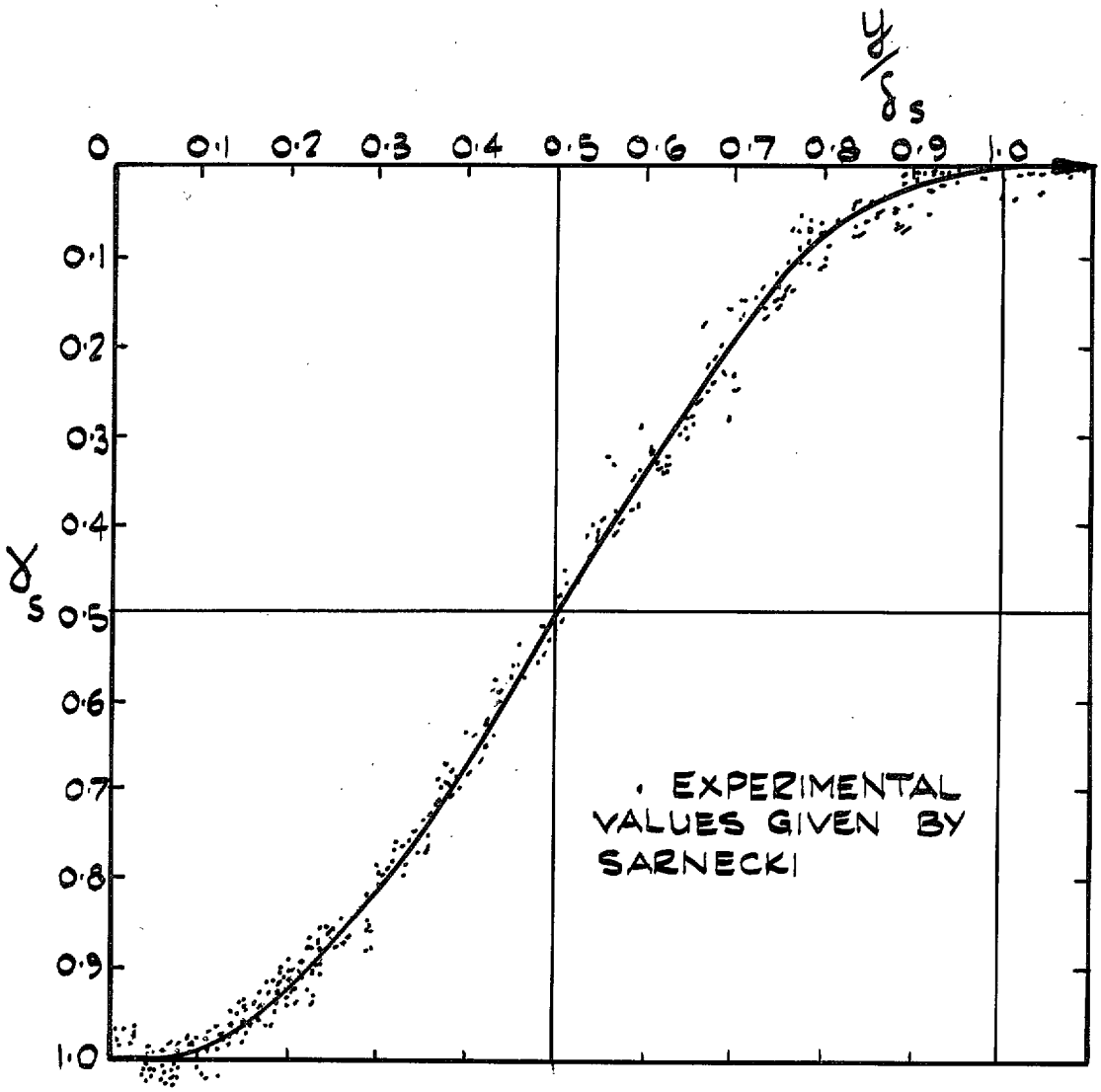

FIG. 5. Choice of mean curve for Sarnecki 'intermittency' correlation.

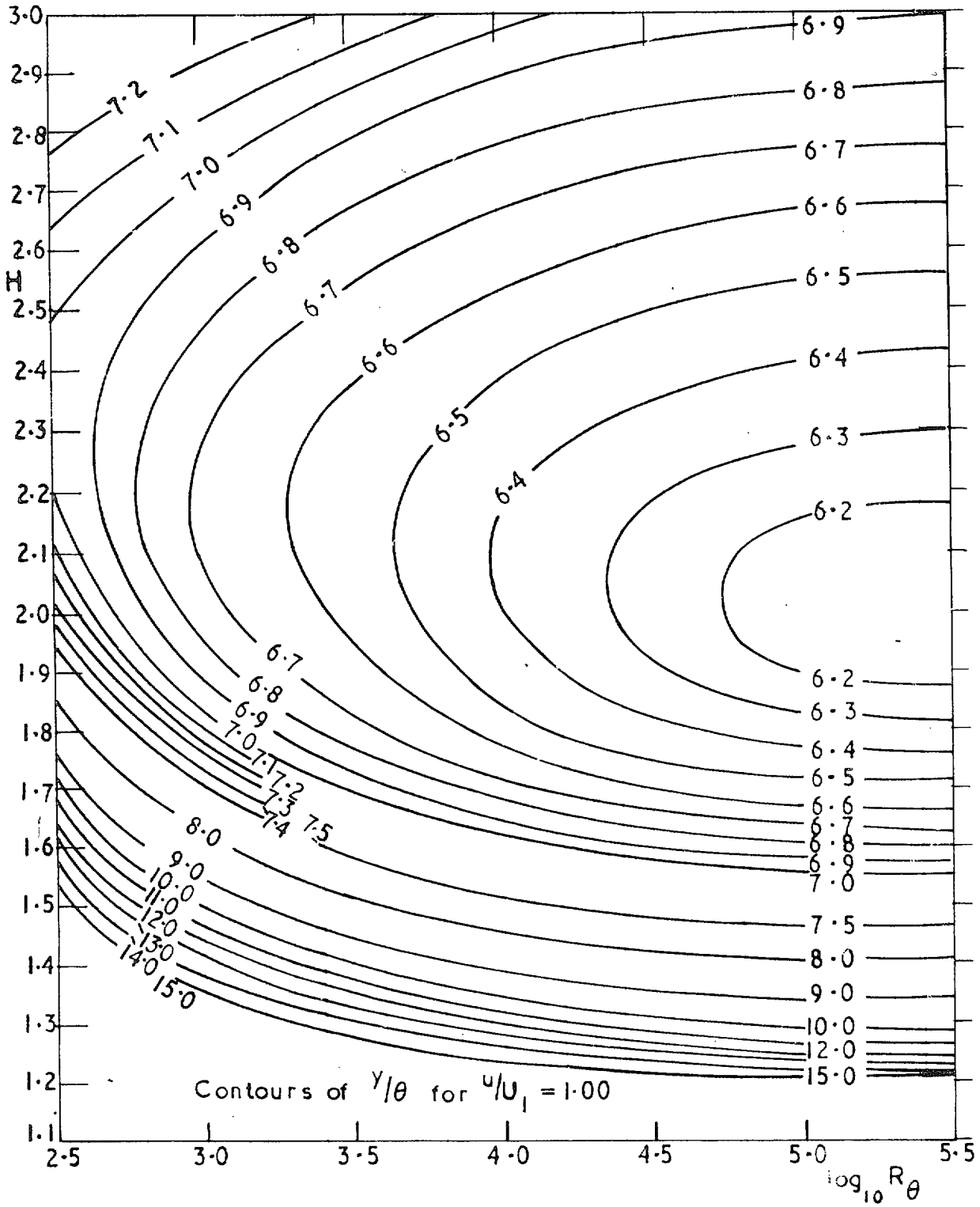

FIG. 6a. Velocity profile chart.

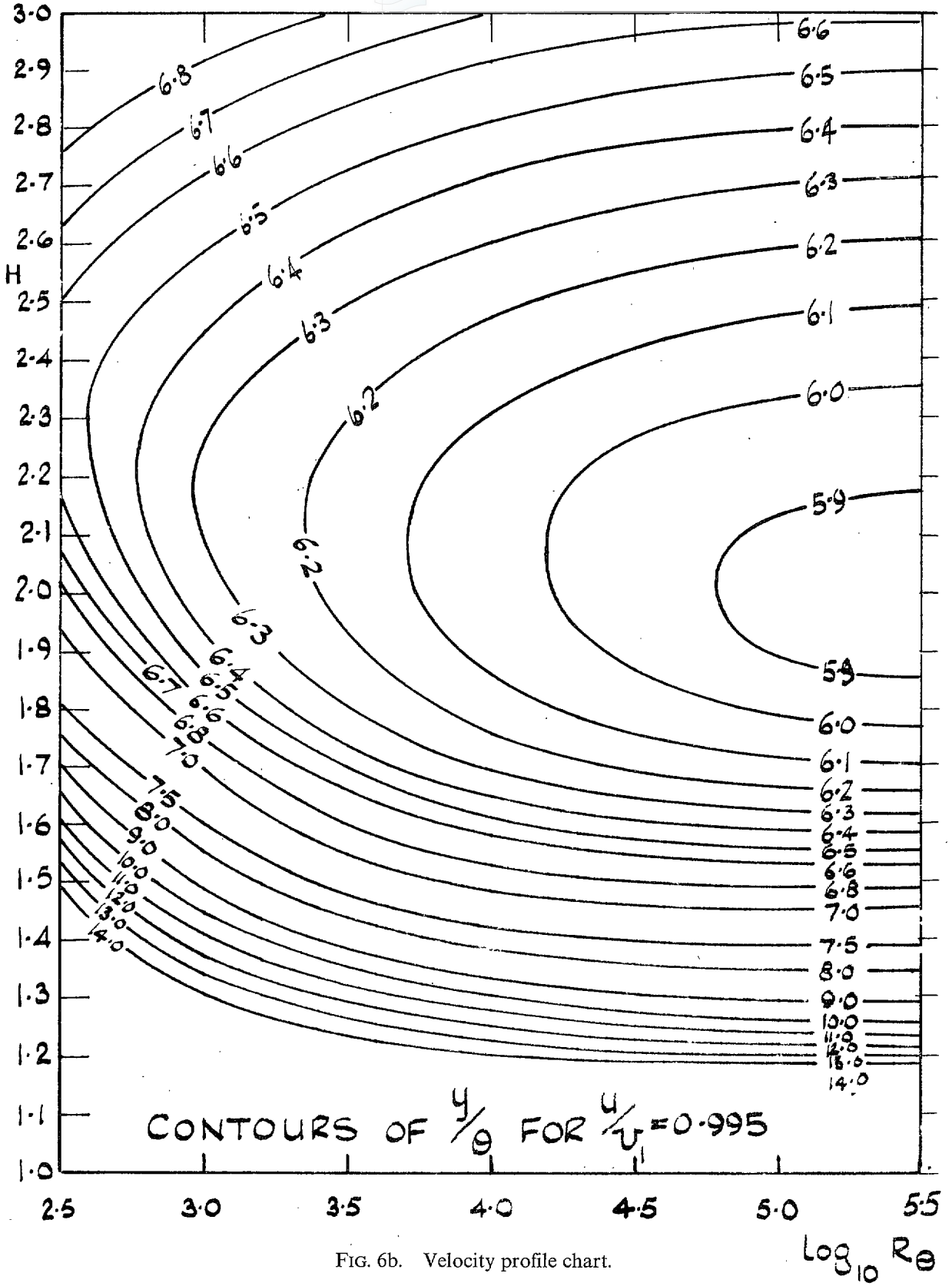

FIG. 6b. Velocity profile chart.

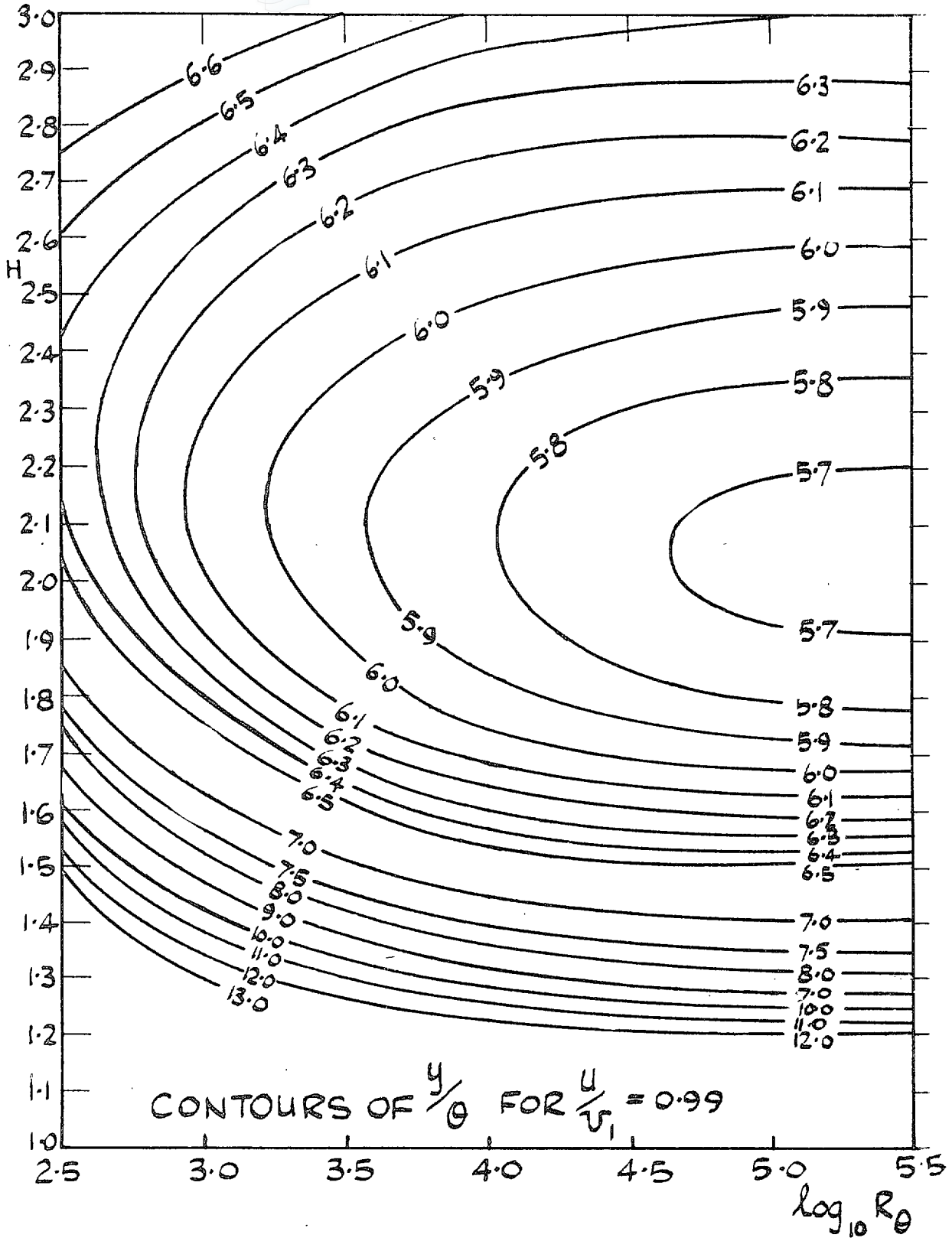

FIG. 6c. Velocity profile chart.

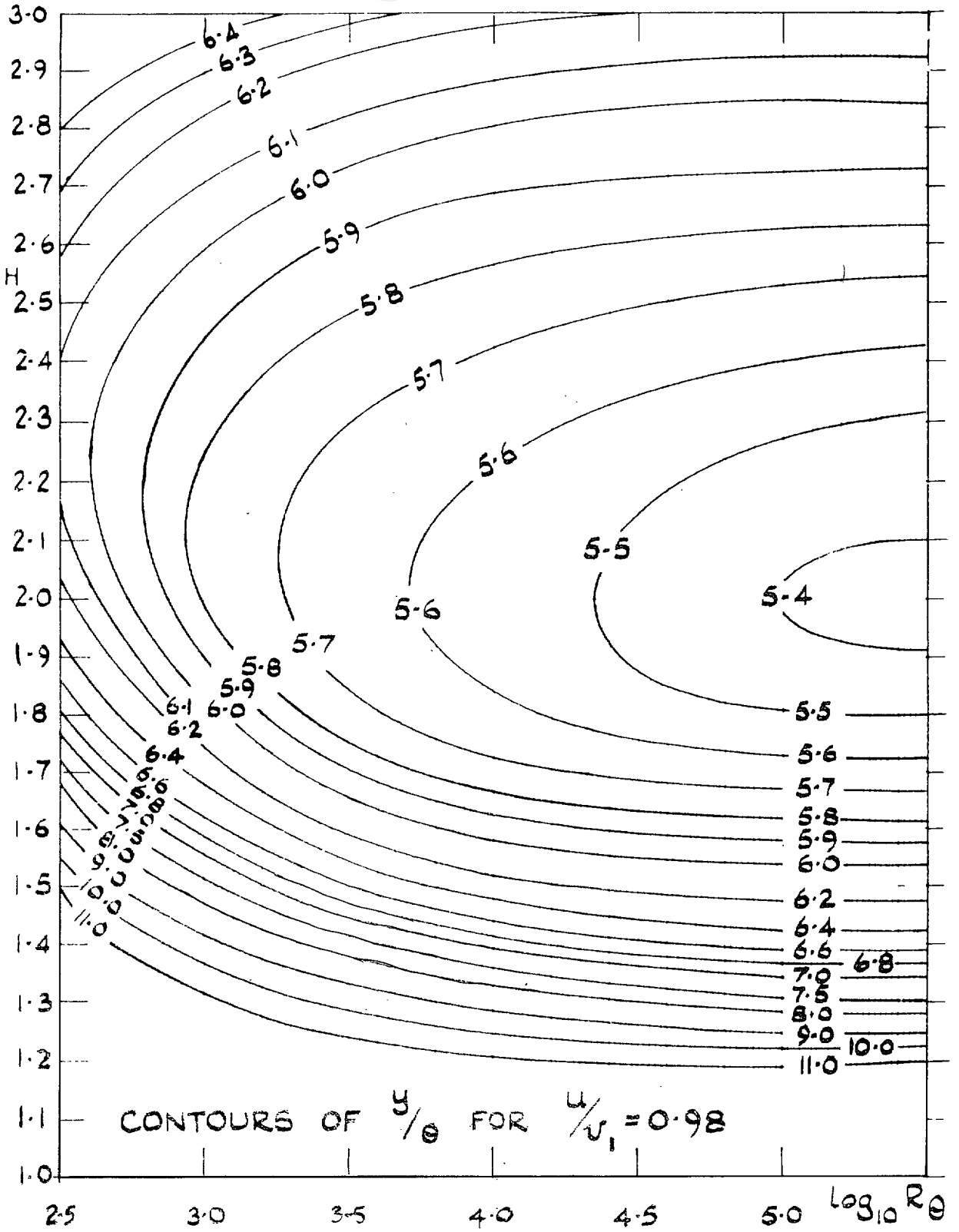

FIG. 6d. Velocity profile chart.

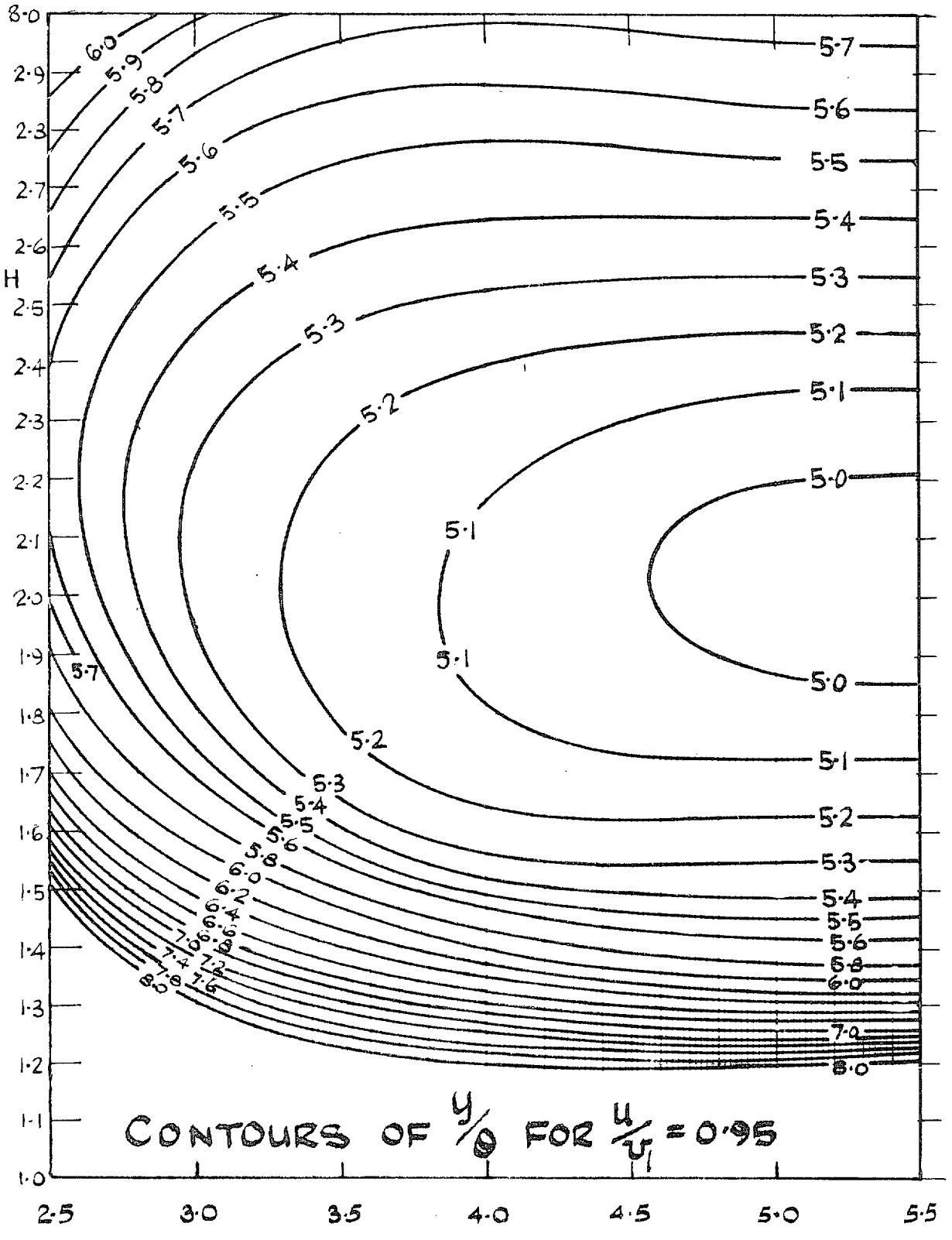

FIG. 6e. Velocity profile chart.

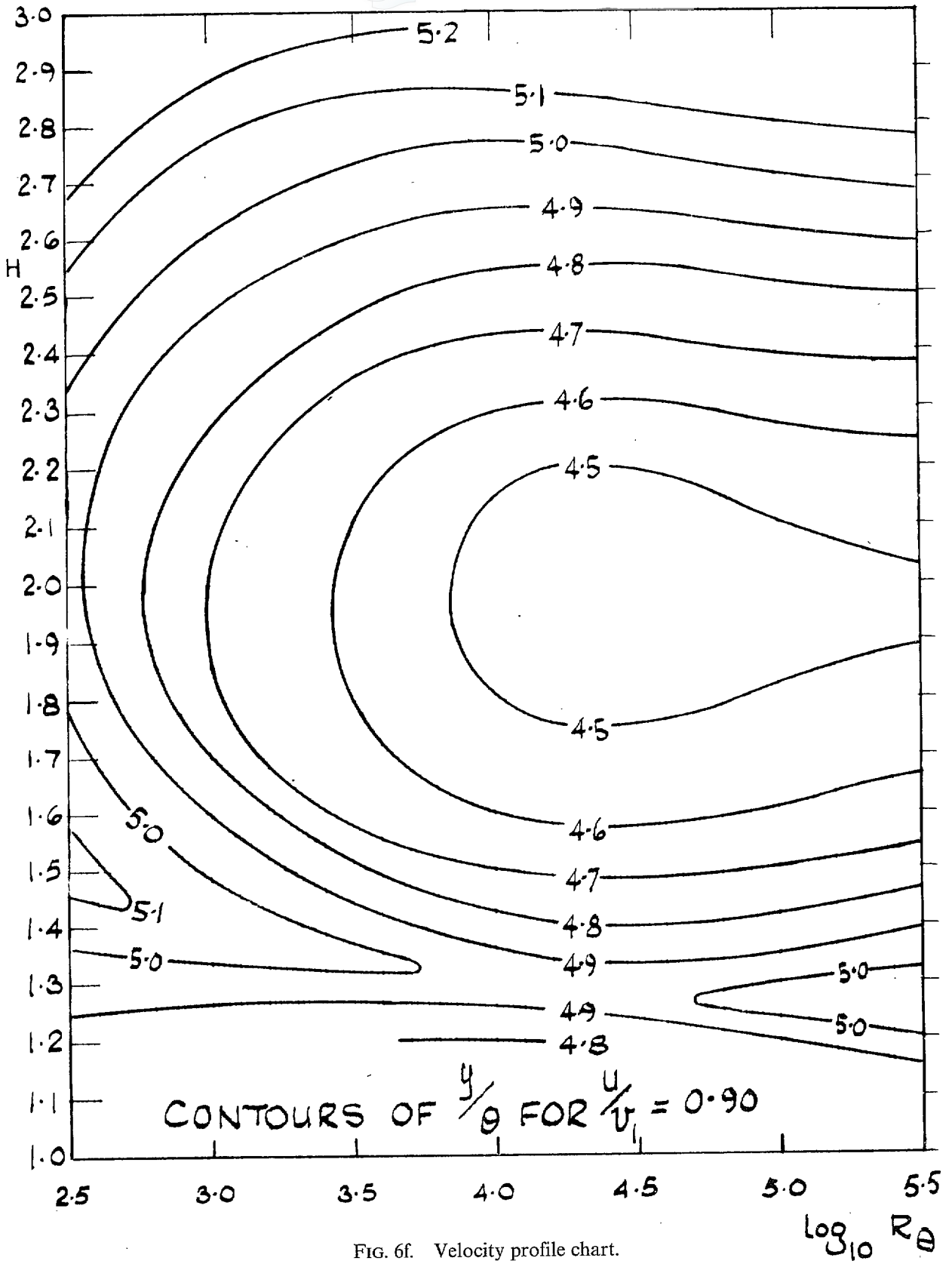

FIG. 6f. Velocity profile chart.

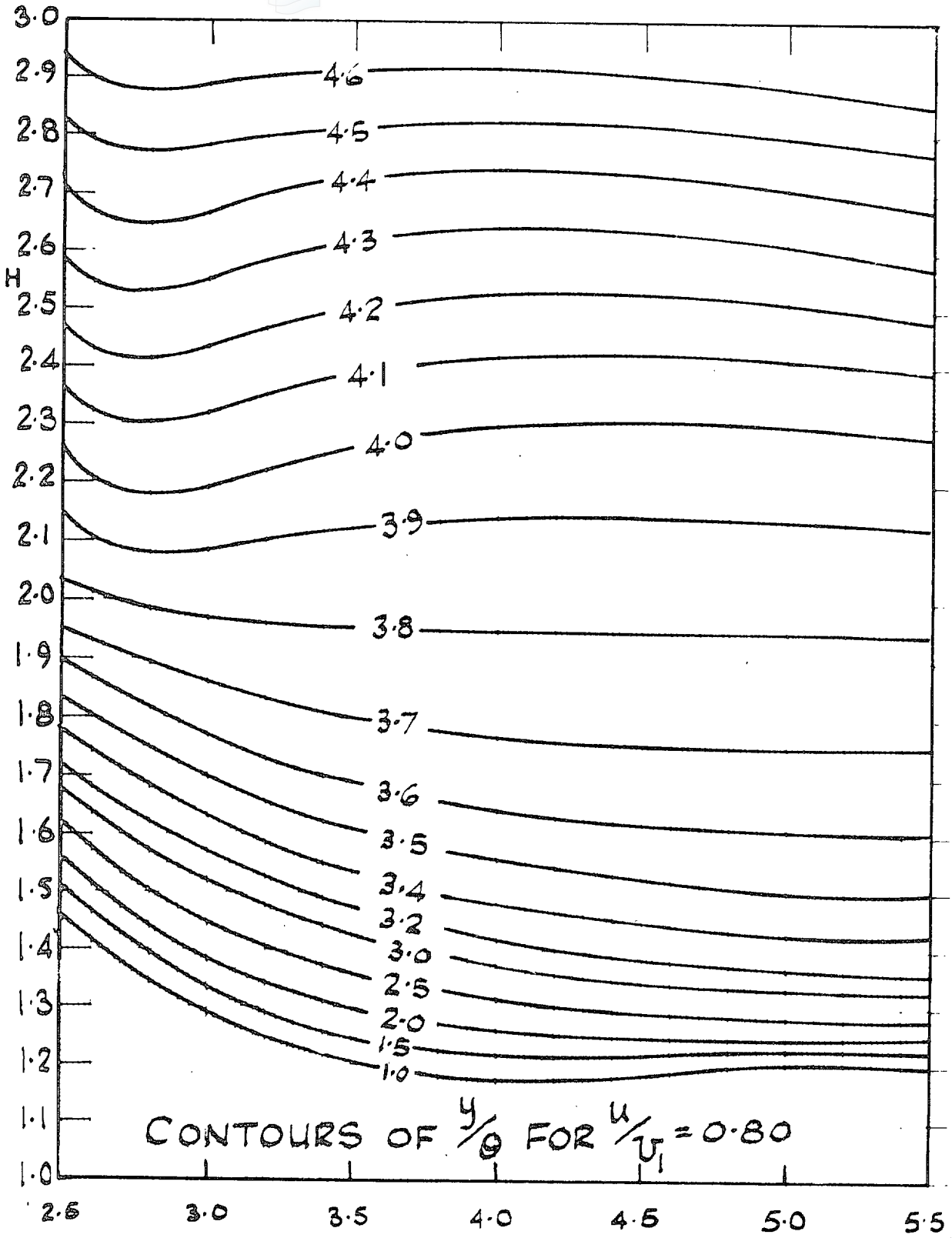

FIG. 6g. Velocity profile chart.

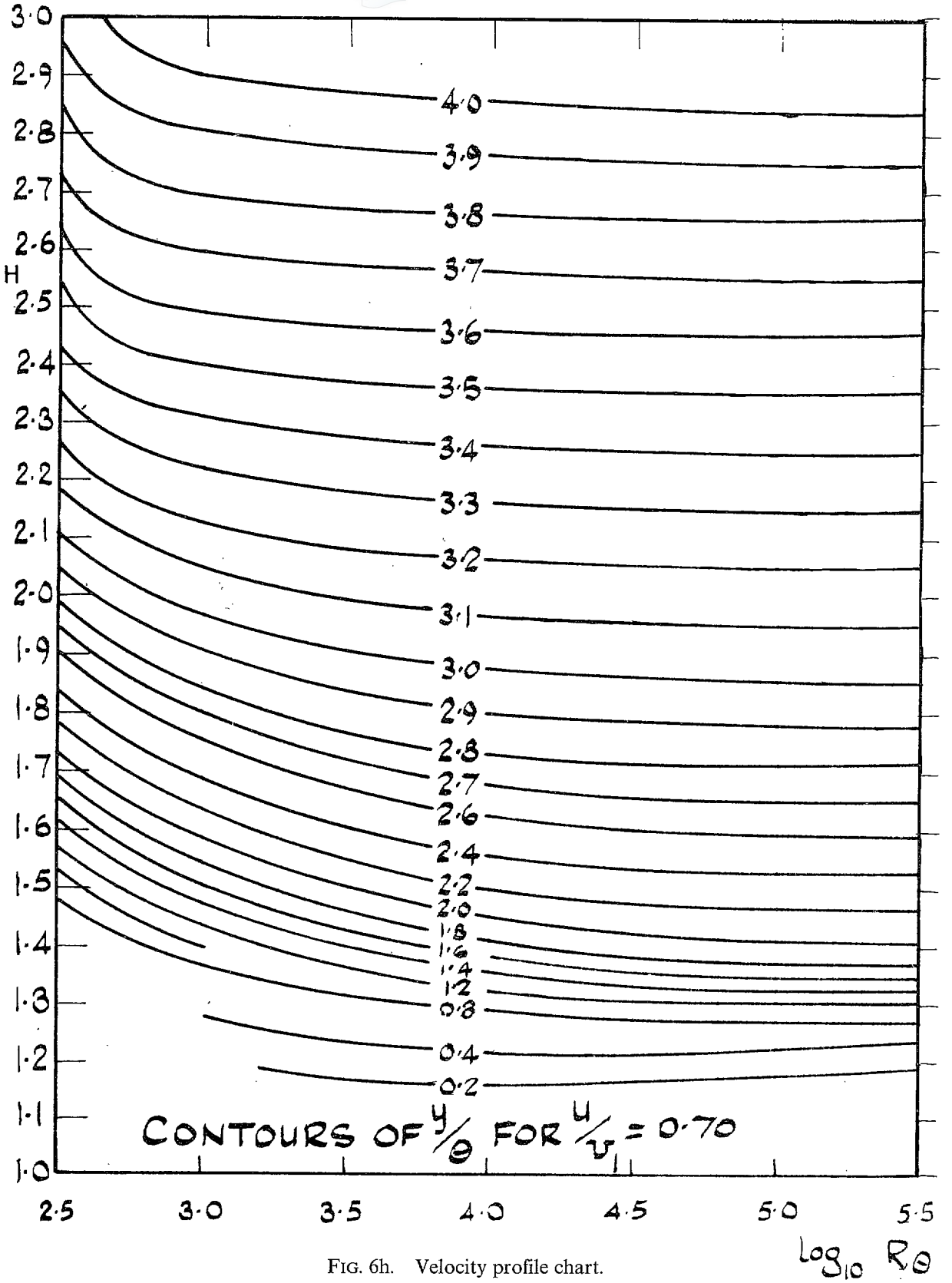

FIG. 6h. Velocity profile chart.

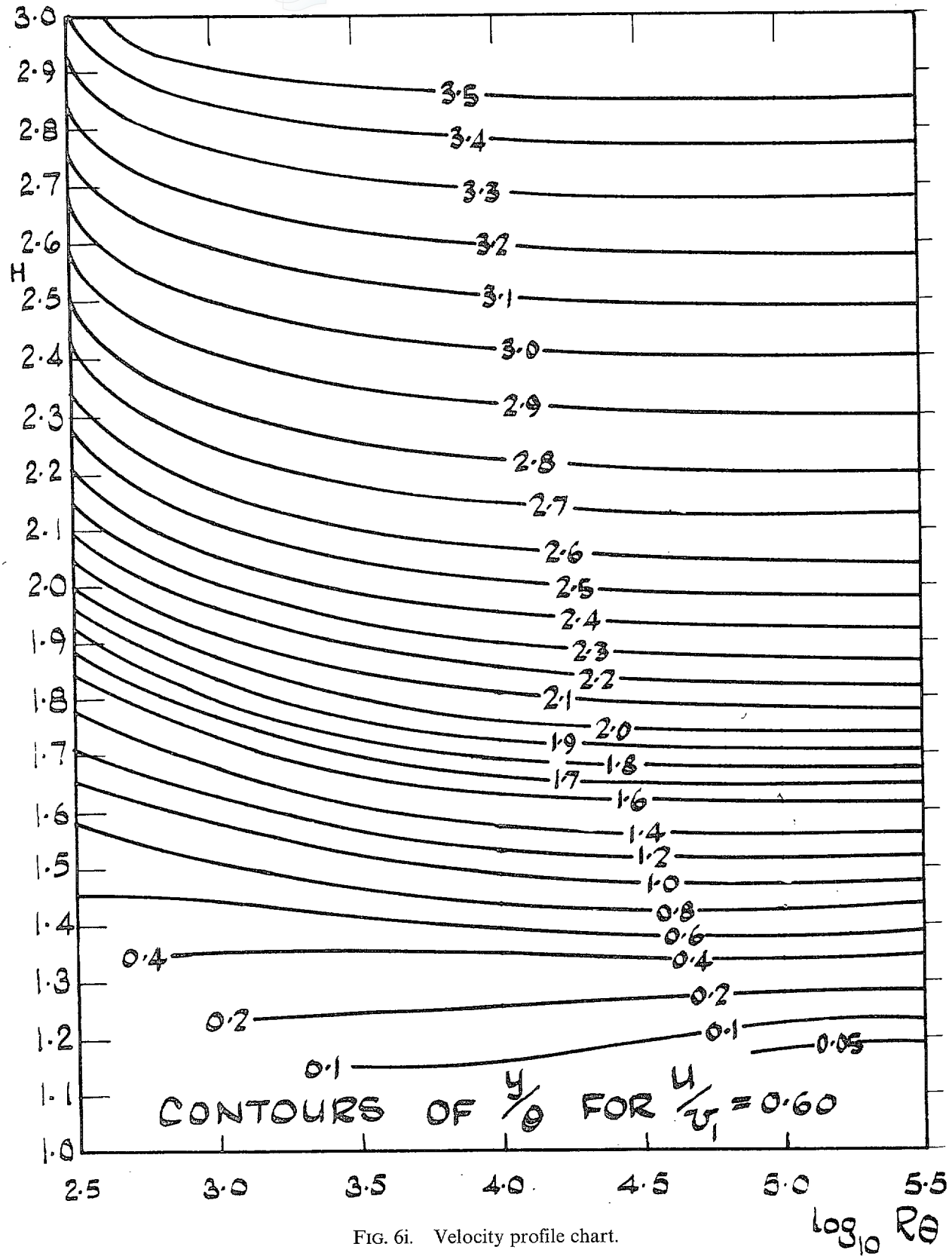

FIG. 6i. Velocity profile chart.

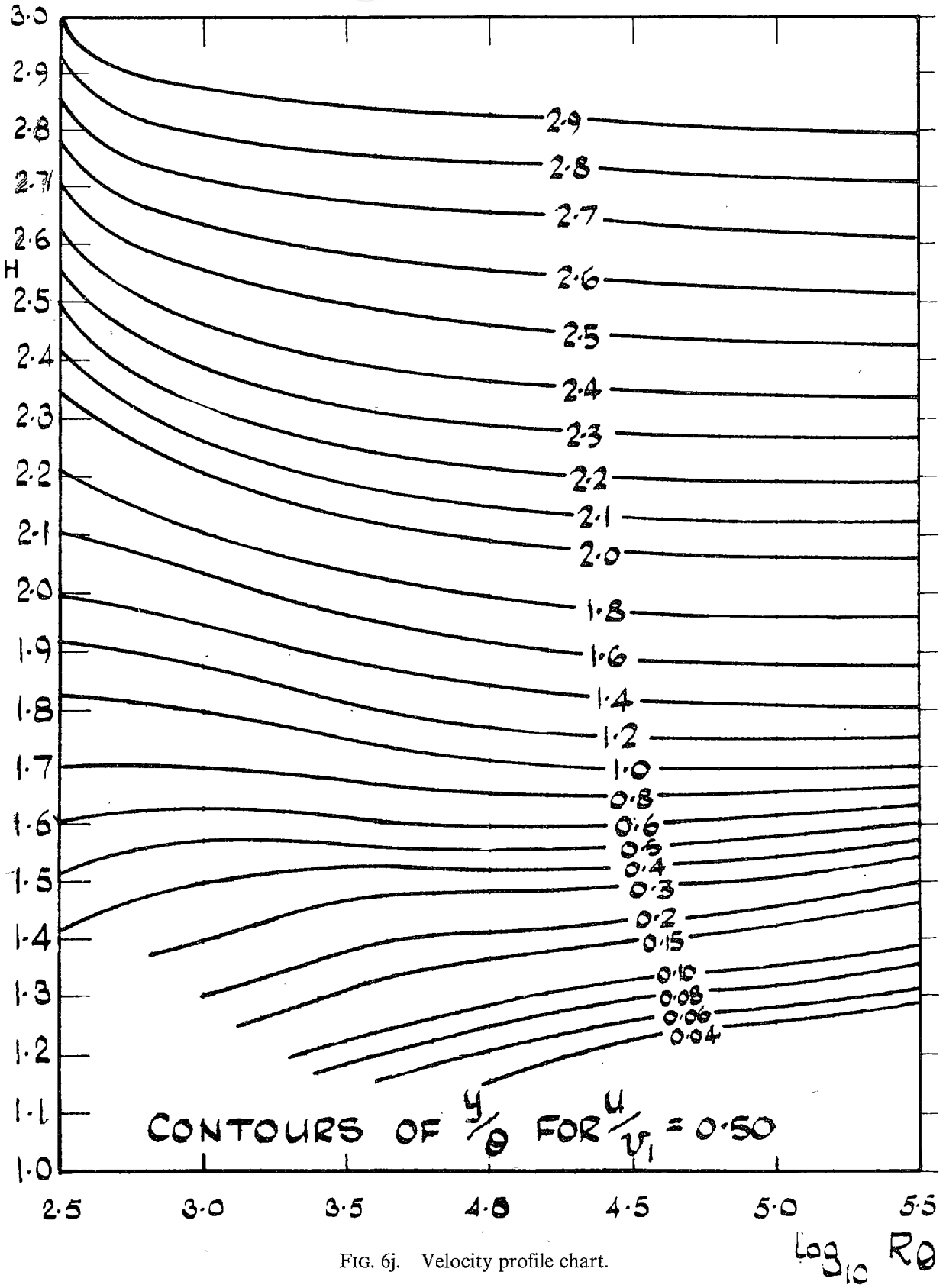

FIG. 6j. Velocity profile chart.

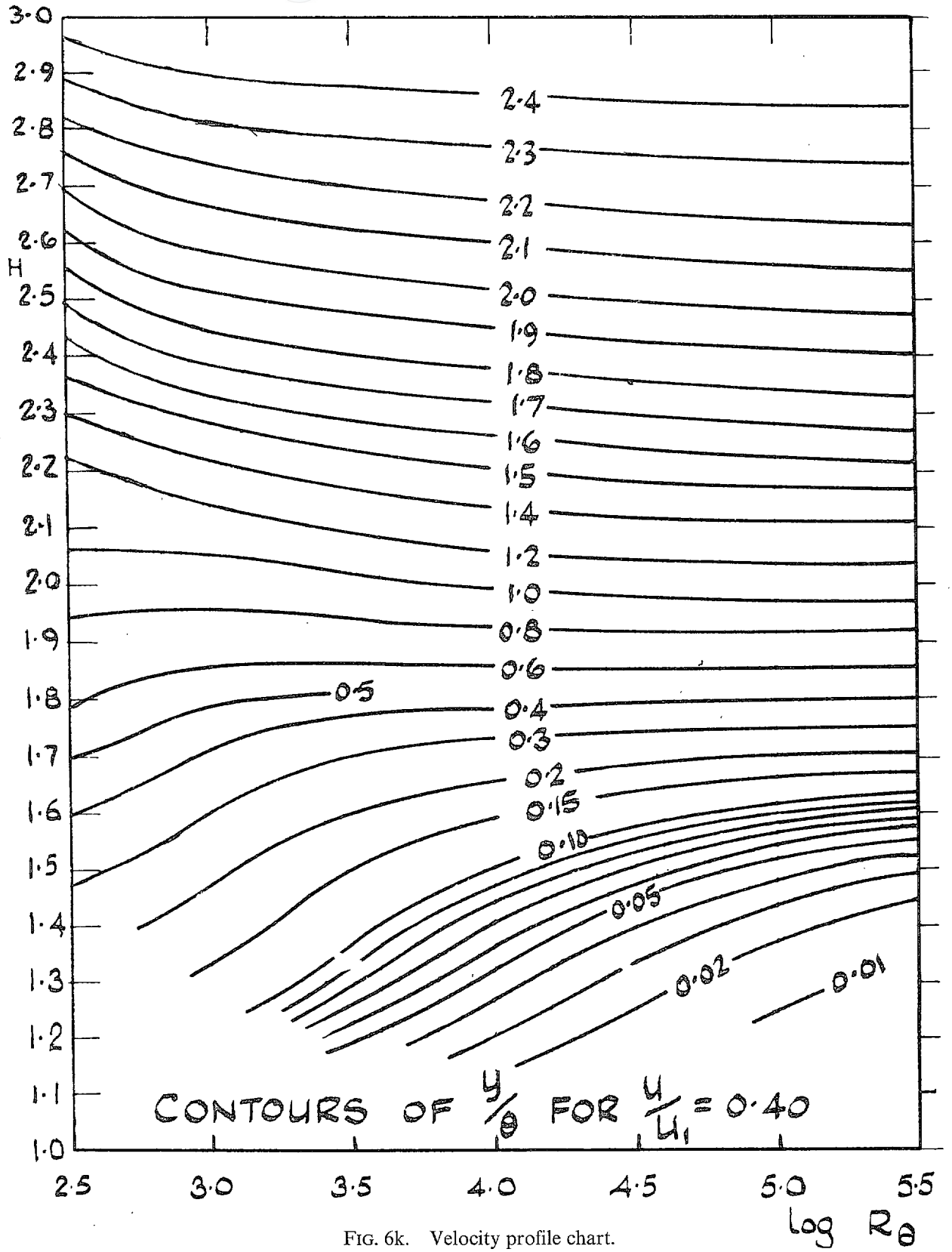

FIG. 6k. Velocity profile chart.

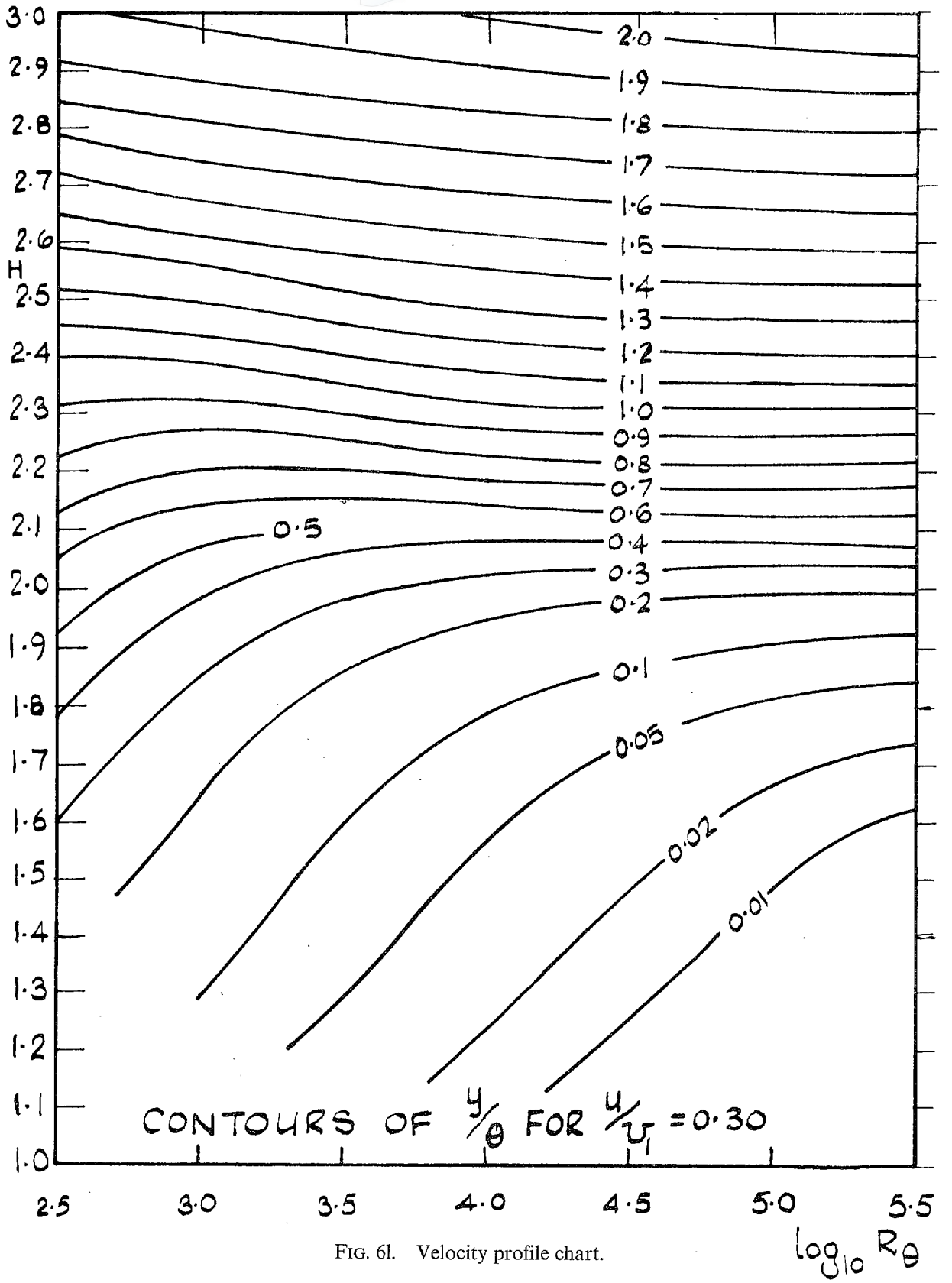

FIG. 6l. Velocity profile chart.

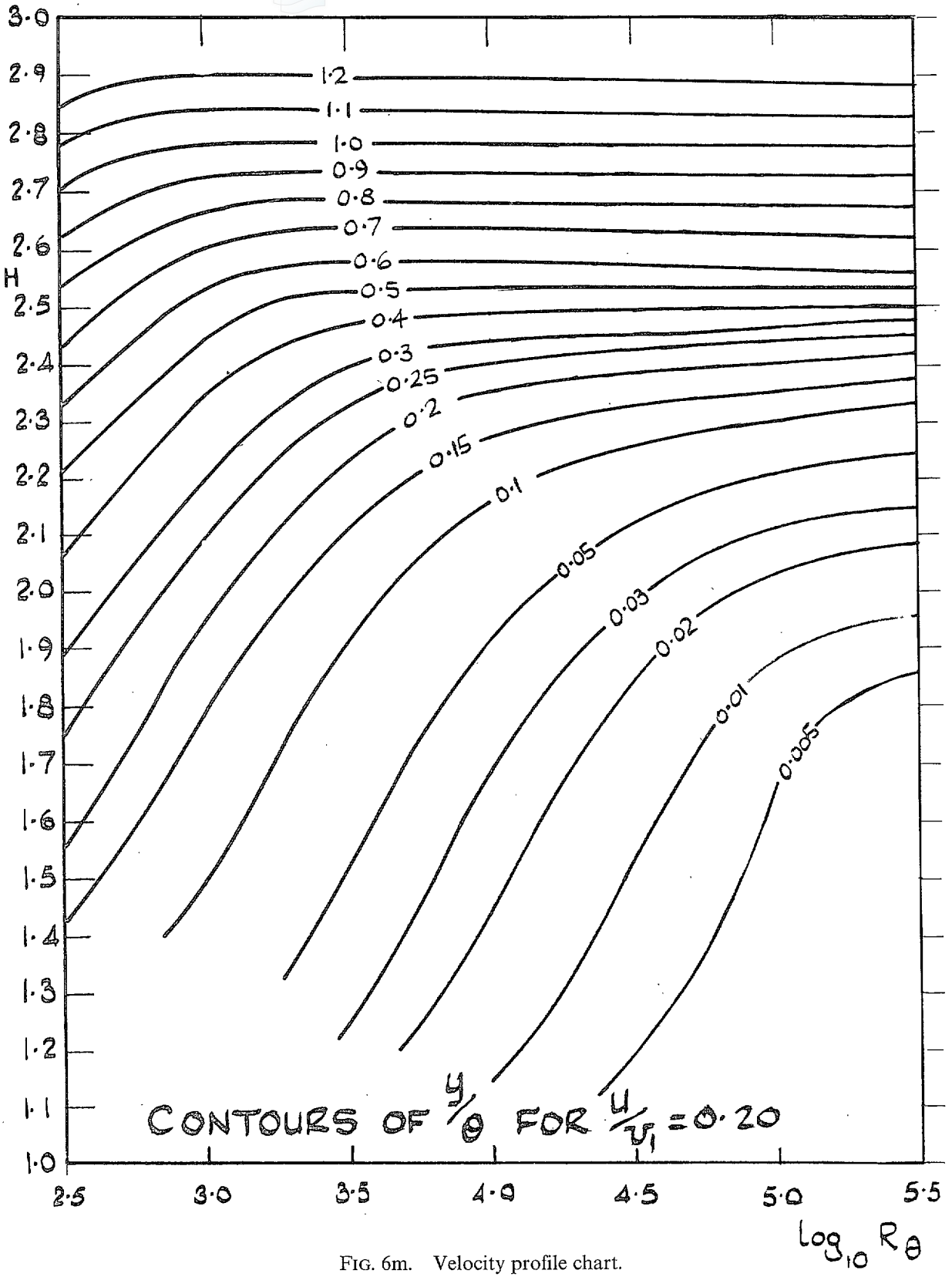

FIG. 6m. Velocity profile chart.

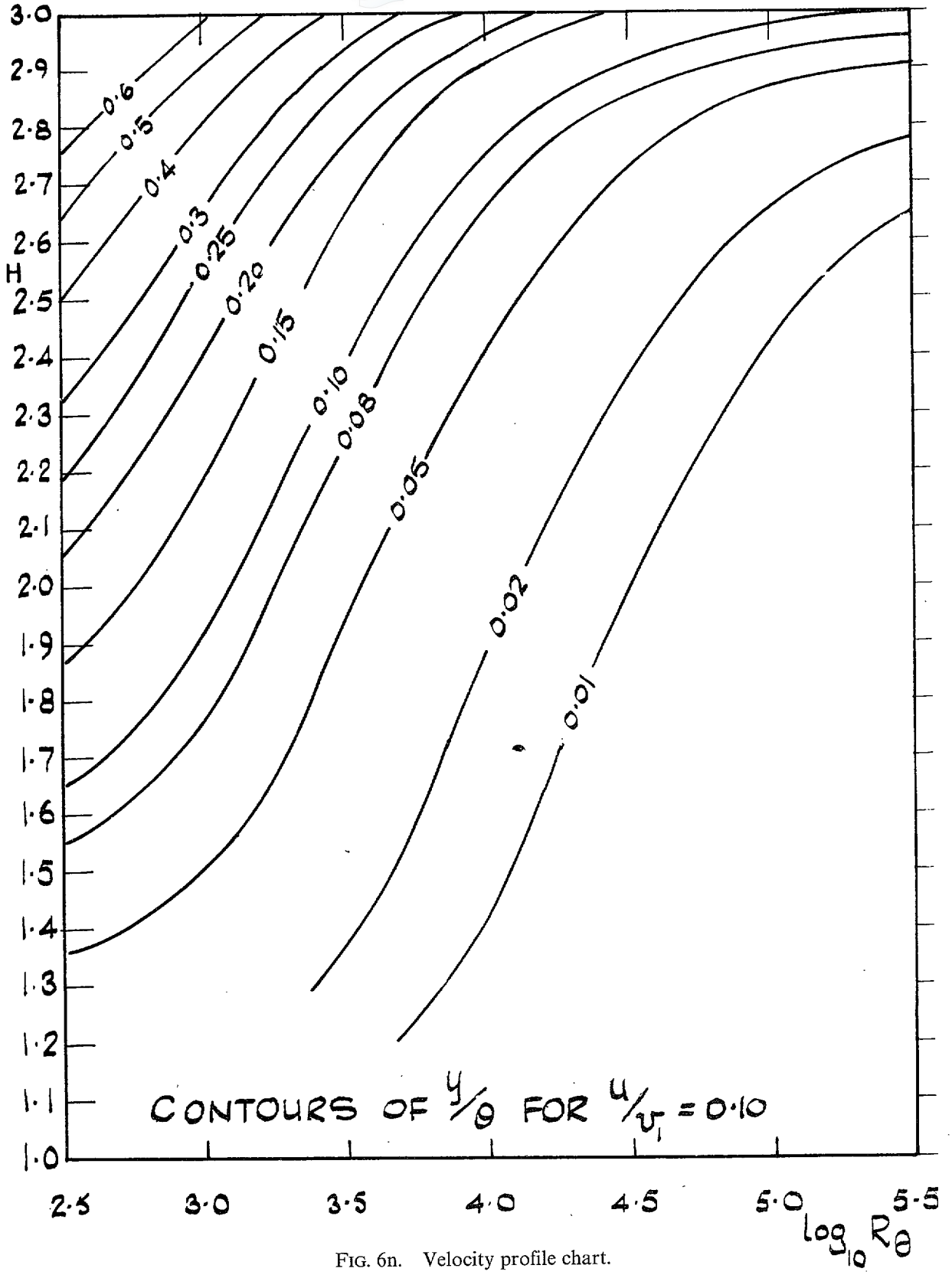

FIG. 6n. Velocity profile chart.

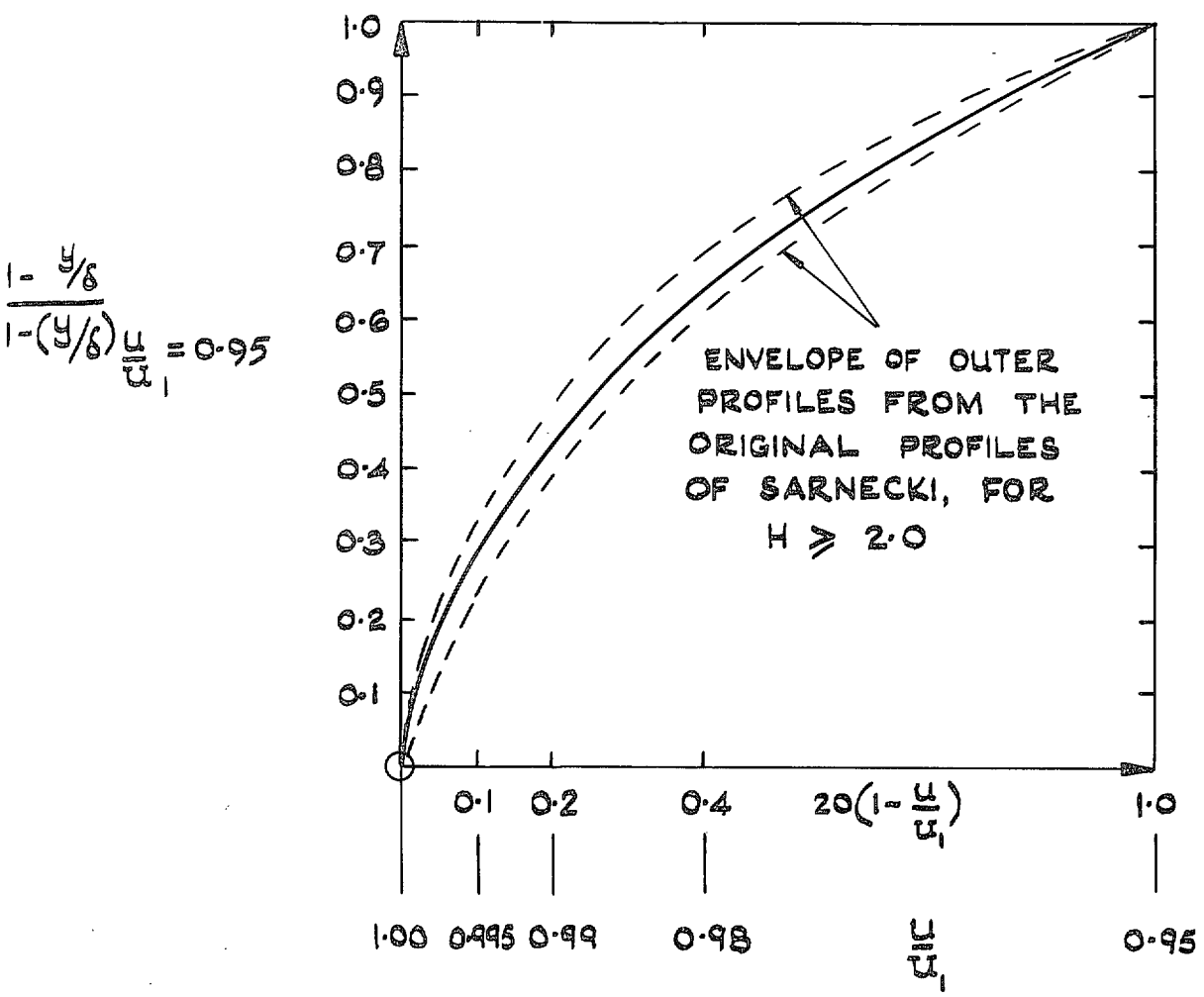

FIG. 7. The universal outer region velocity defect profile.

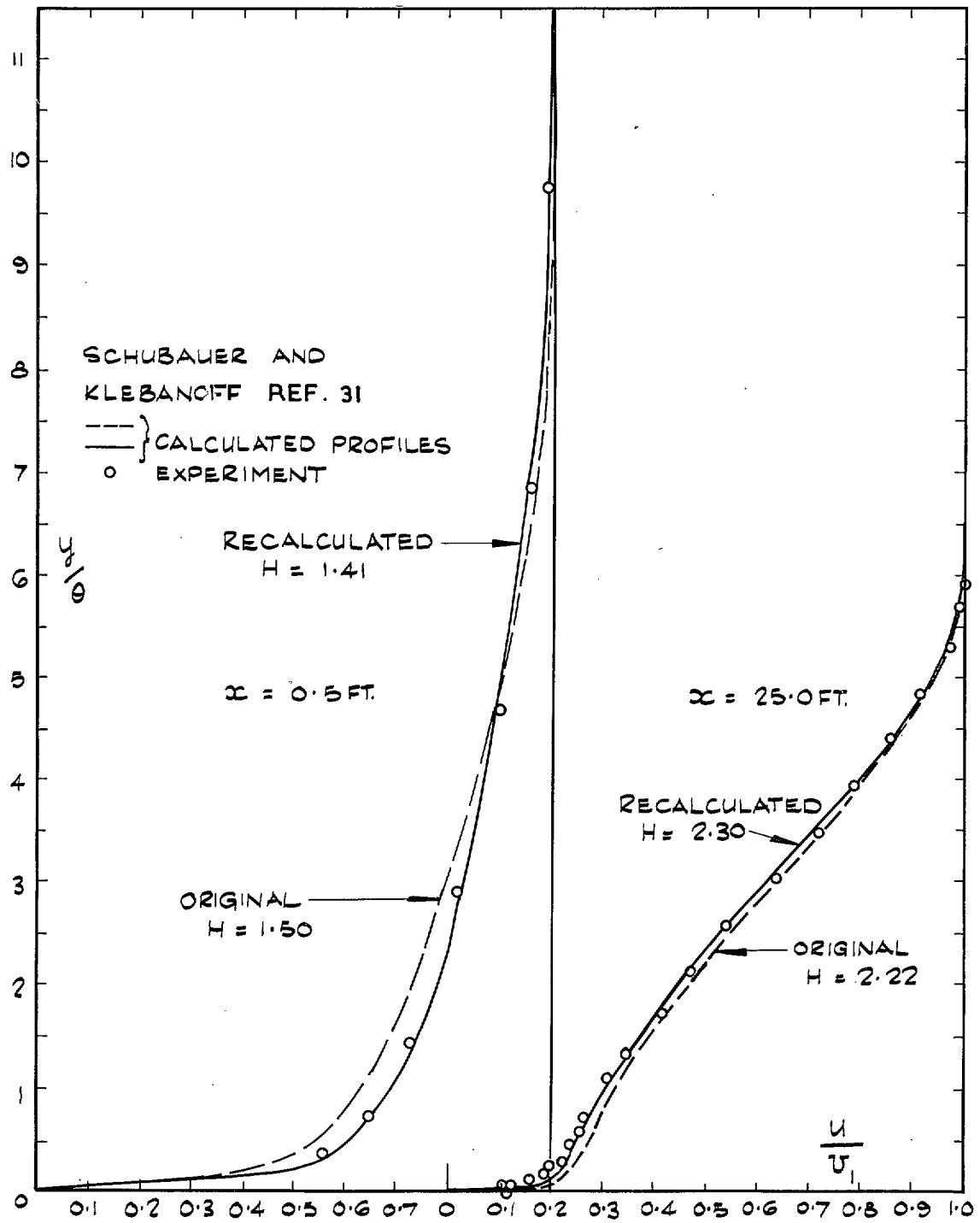

FIG. 8. Profile comparisons on the basis of published and recalculated values for H, R_θ.

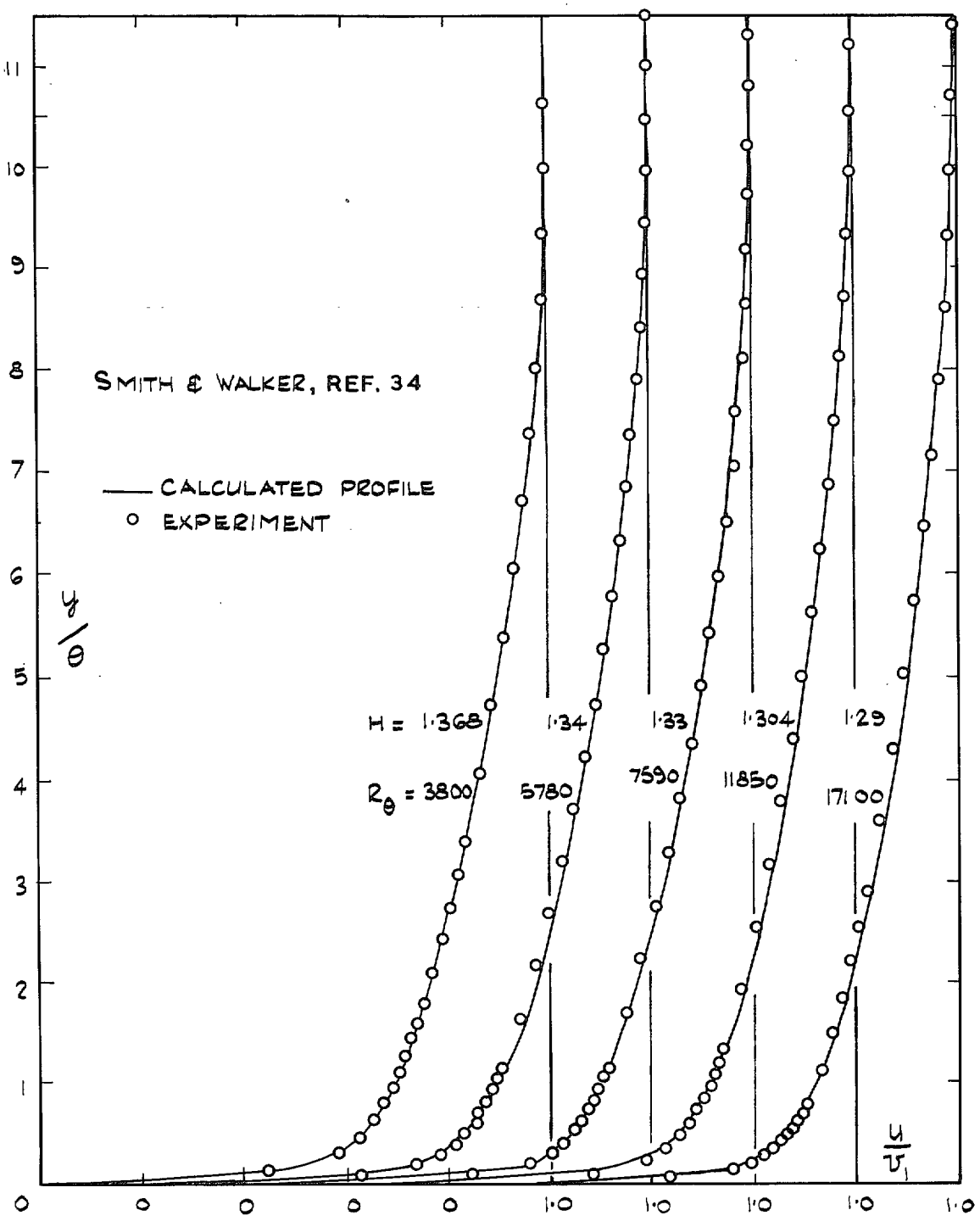

FIG. 9. Comparison of the new family mean velocity profiles with experiment.

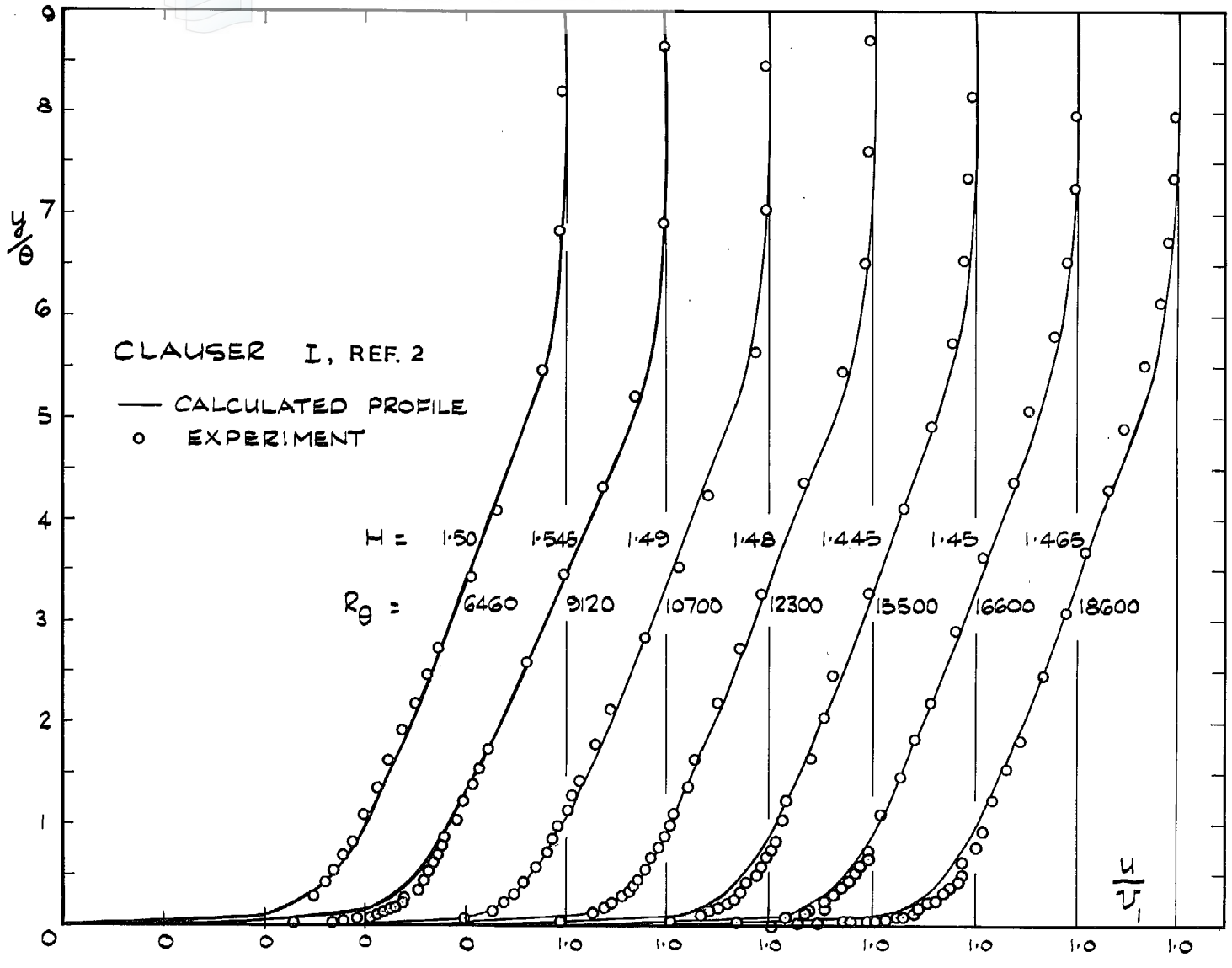

FIG. 10. Comparison of the new family of mean velocity profiles with experiments.

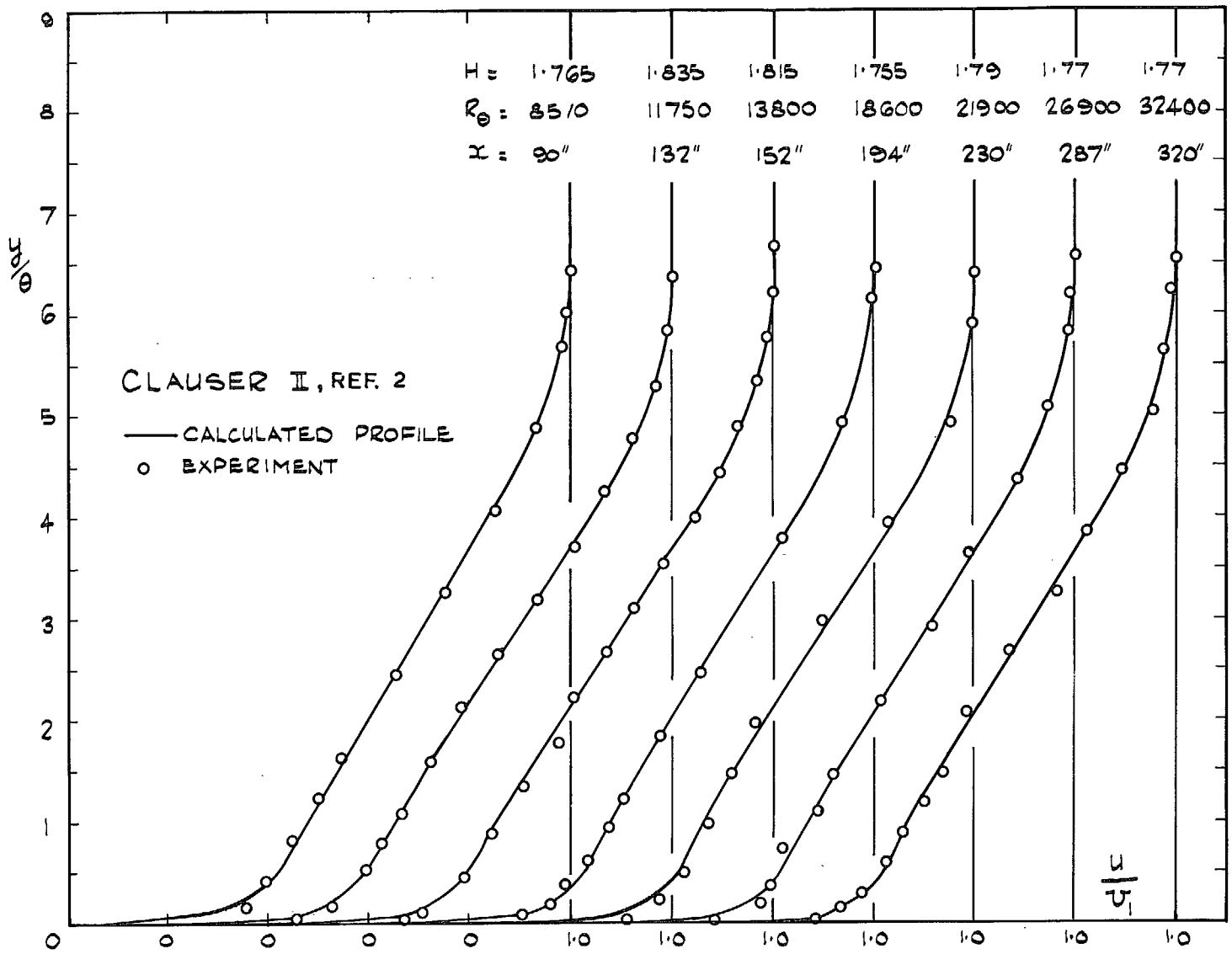

FIG. 11. Comparison of the new family of mean velocity profiles with experiment.

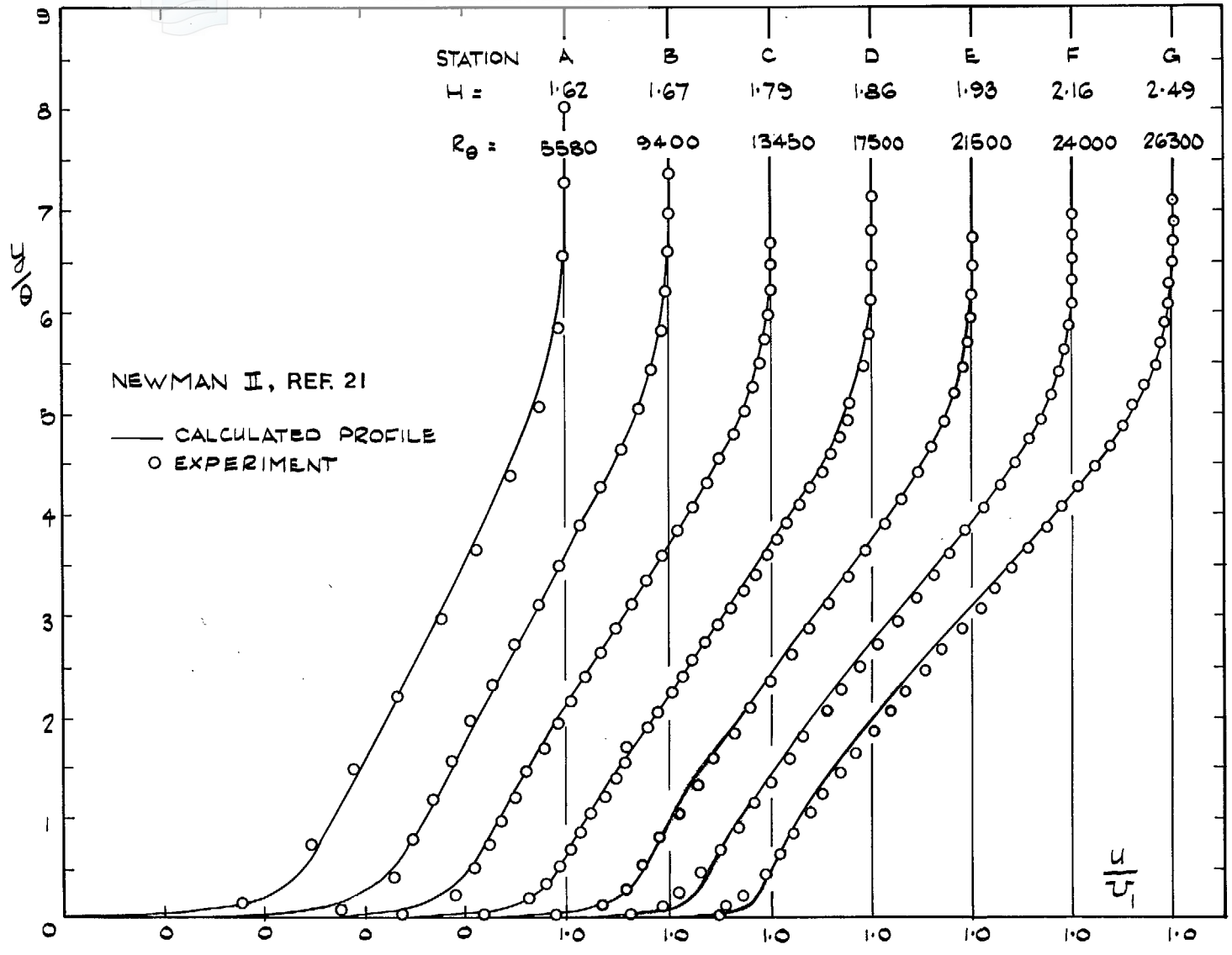

FIG. 12. Comparison of the new family of mean velocity profiles with experiment.

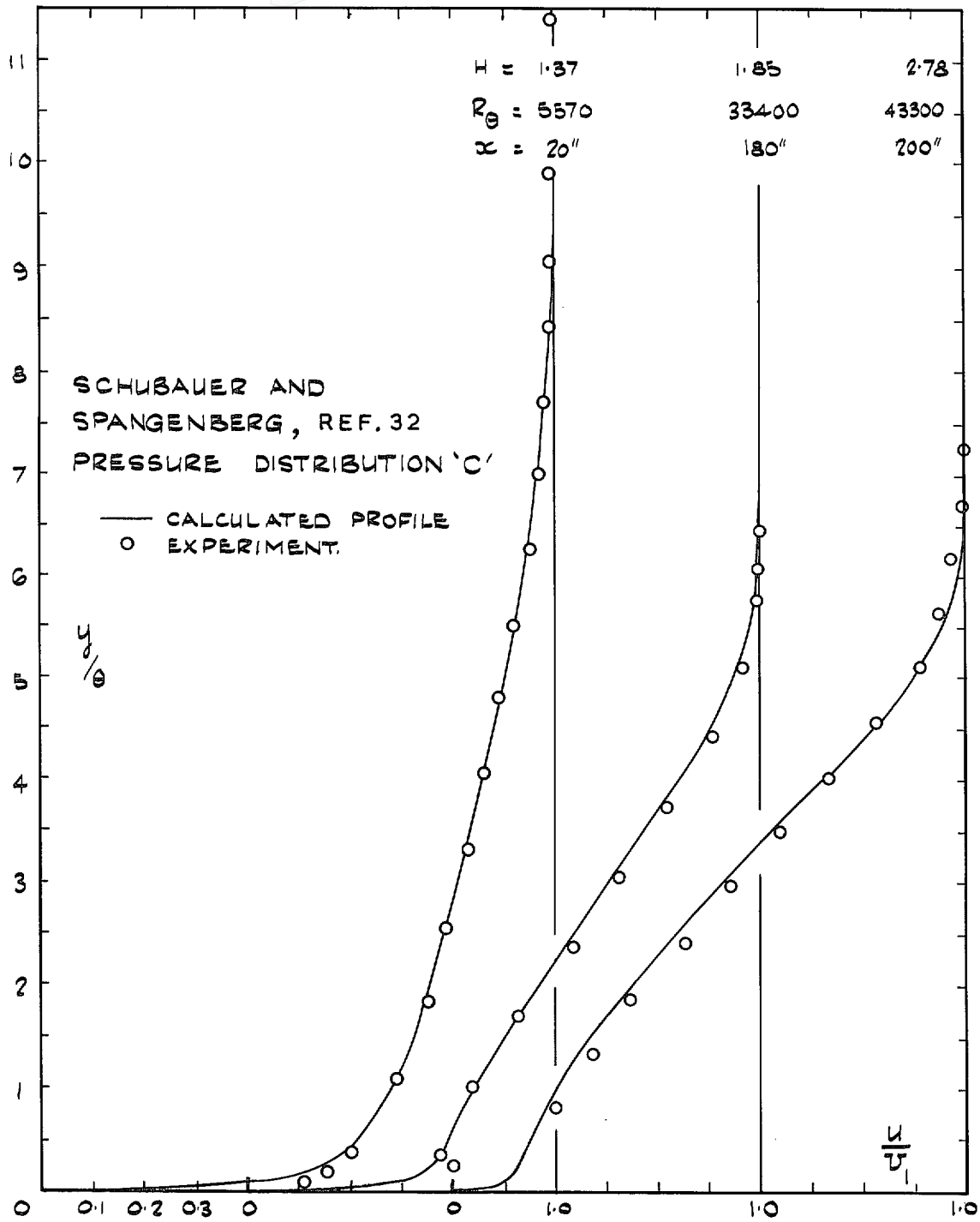

FIG. 13. Comparison of the new family of mean velocity profiles with experiment.

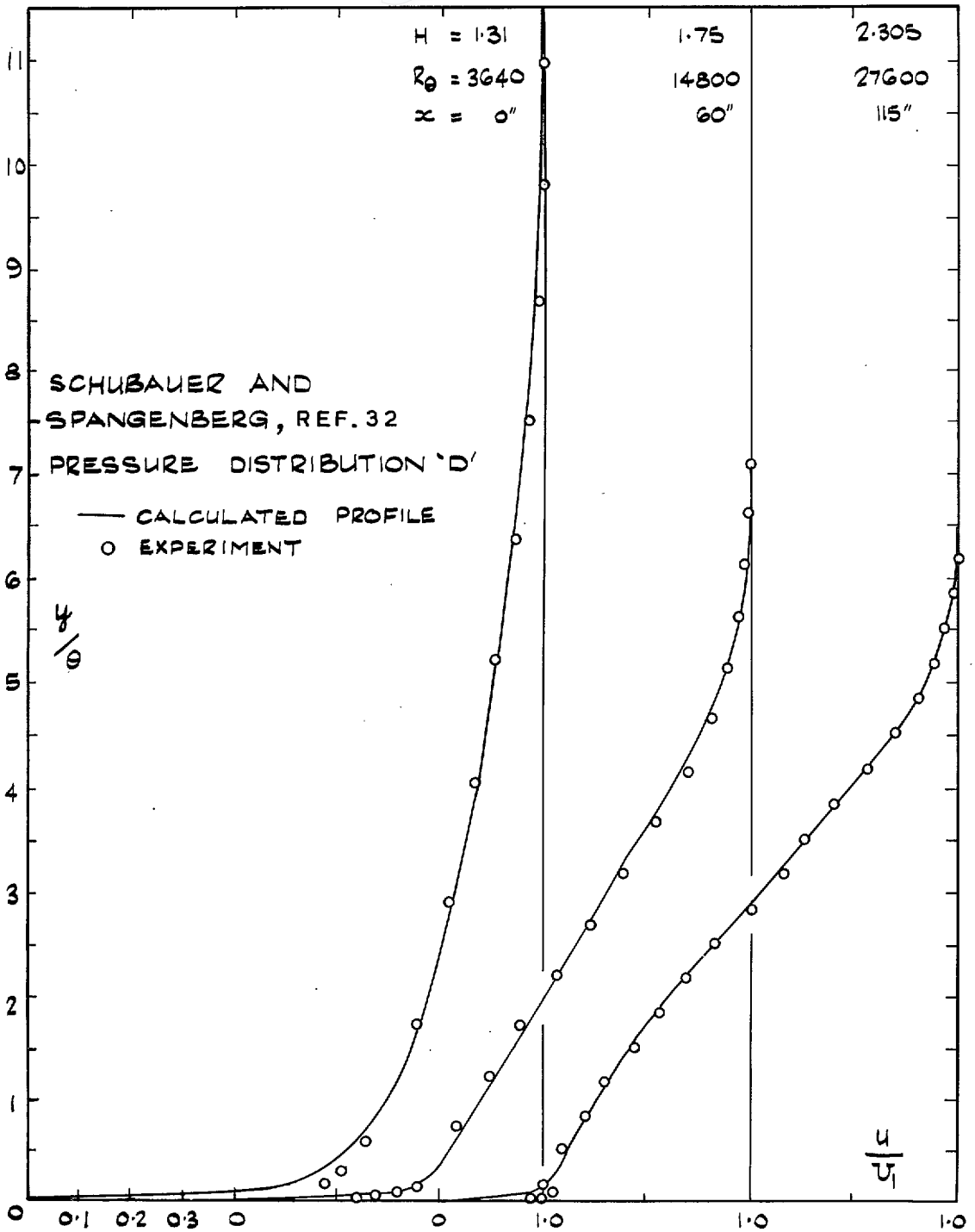

FIG. 14. Comparison of the new family of mean velocity profiles with experiment.

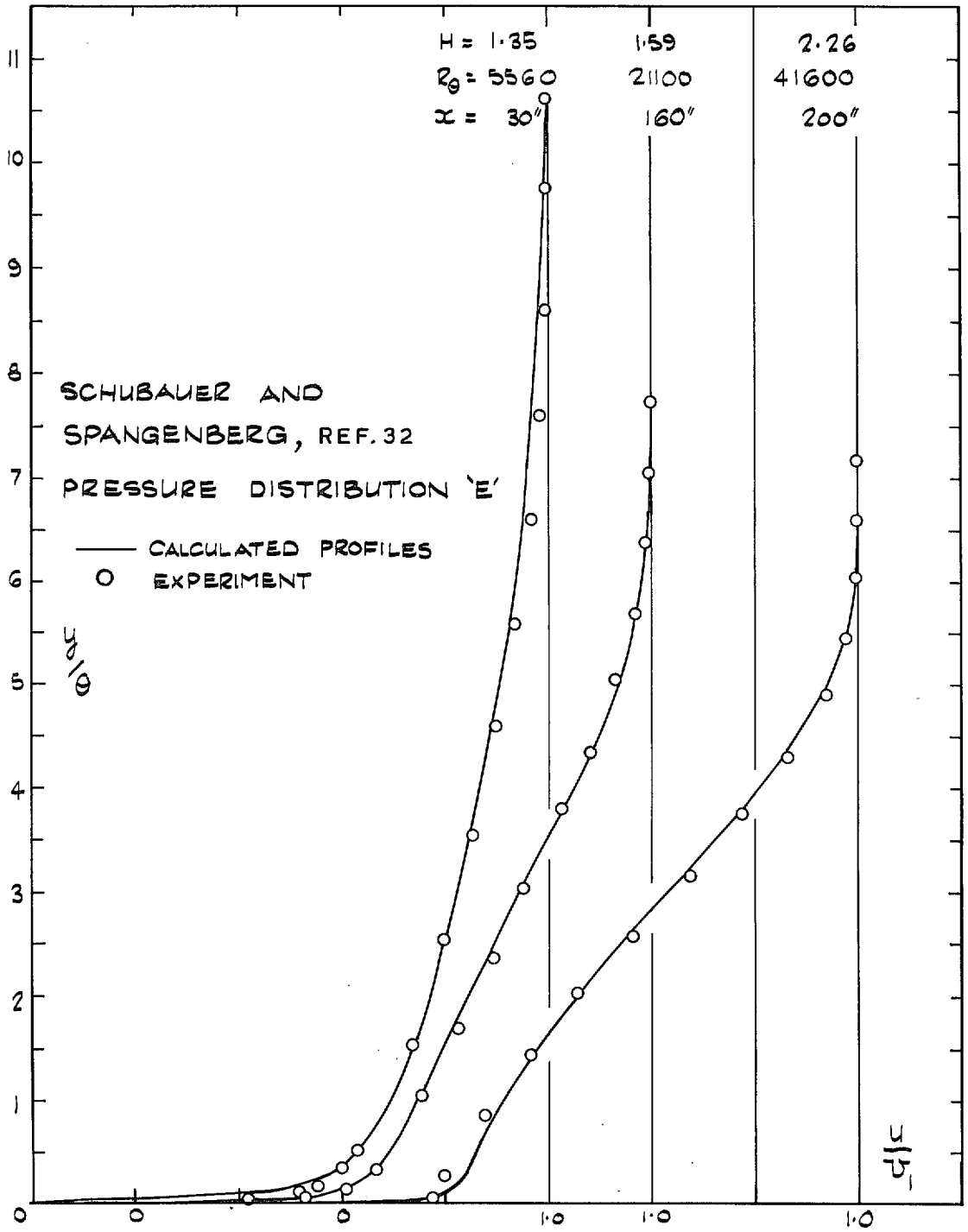

FIG. 15. Comparison of the new family of mean velocity profiles with experiment.

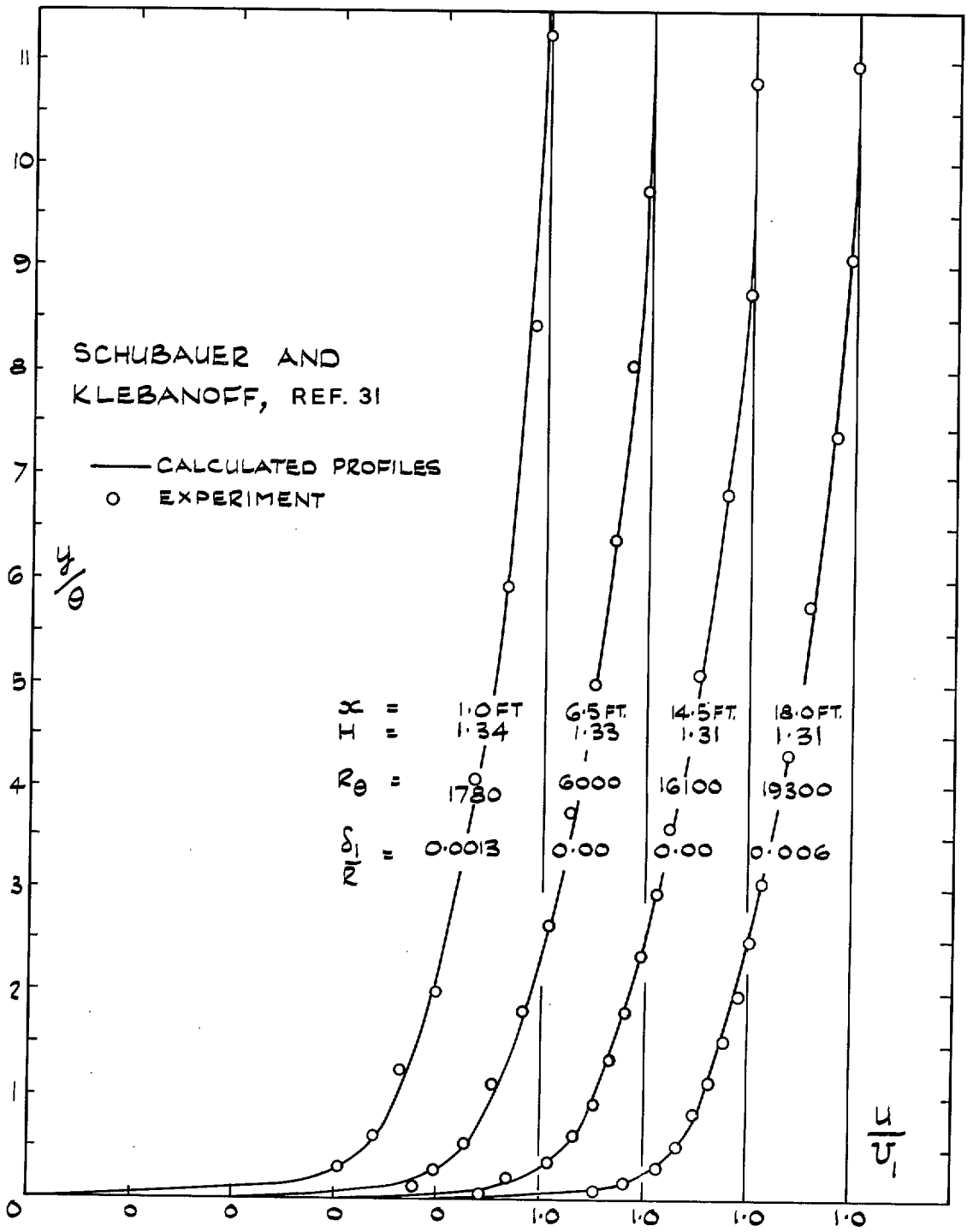

FIG. 16. Comparison of the new family of mean velocity profiles with experiment.

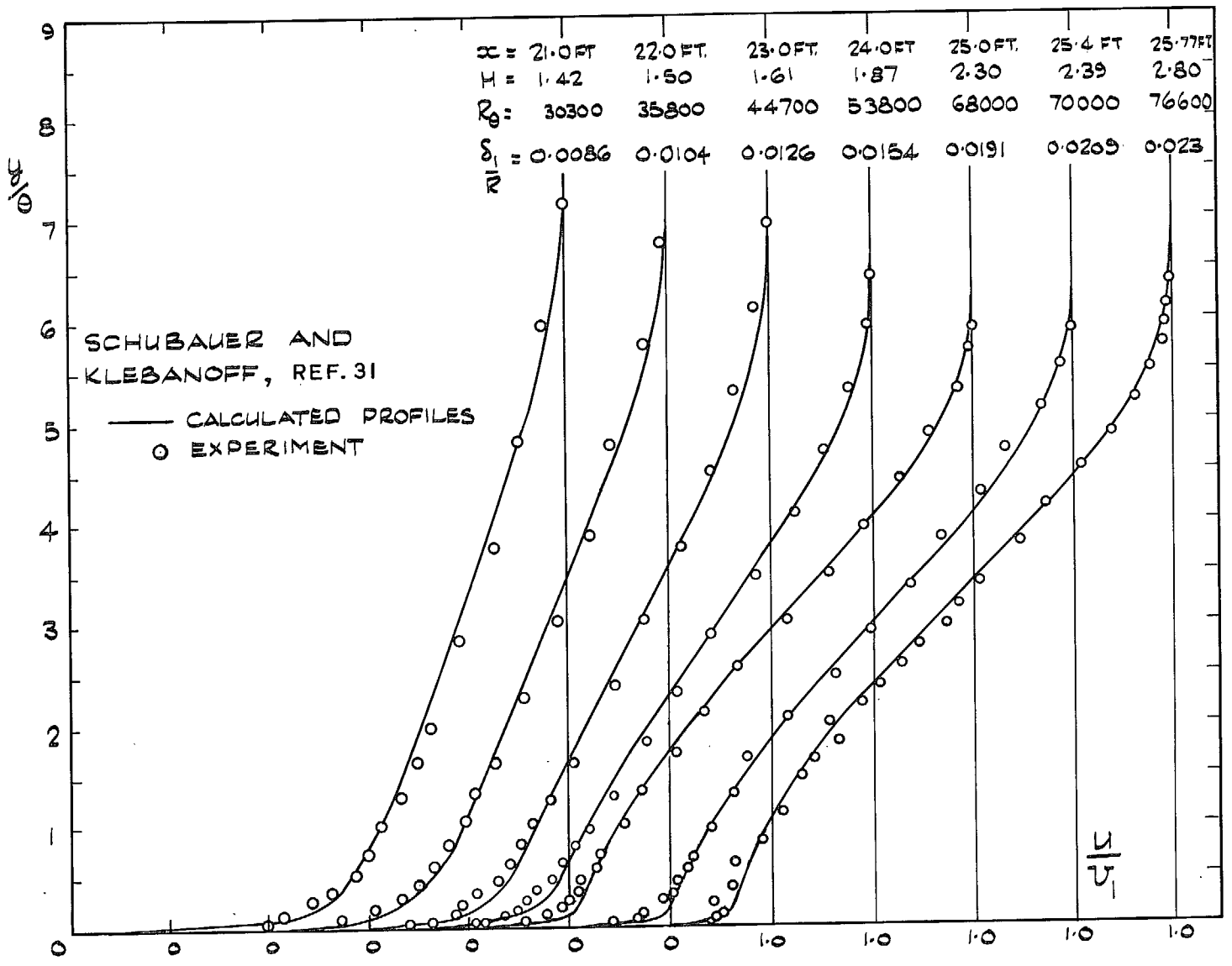

FIG. 17. Comparison of the new family of mean velocity profiles with experiment.

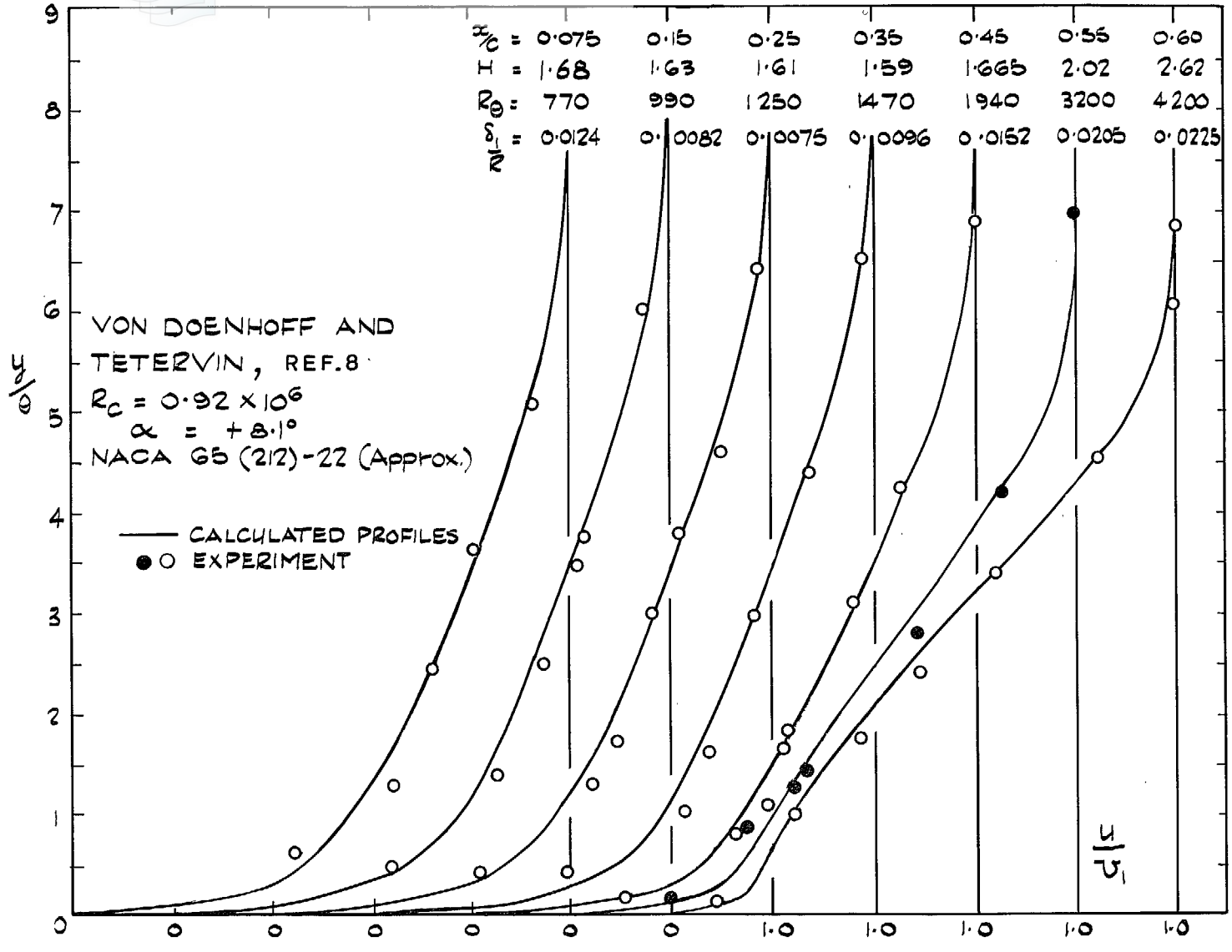

FIG. 18. Comparison of the new family of mean velocity profiles with experiment.

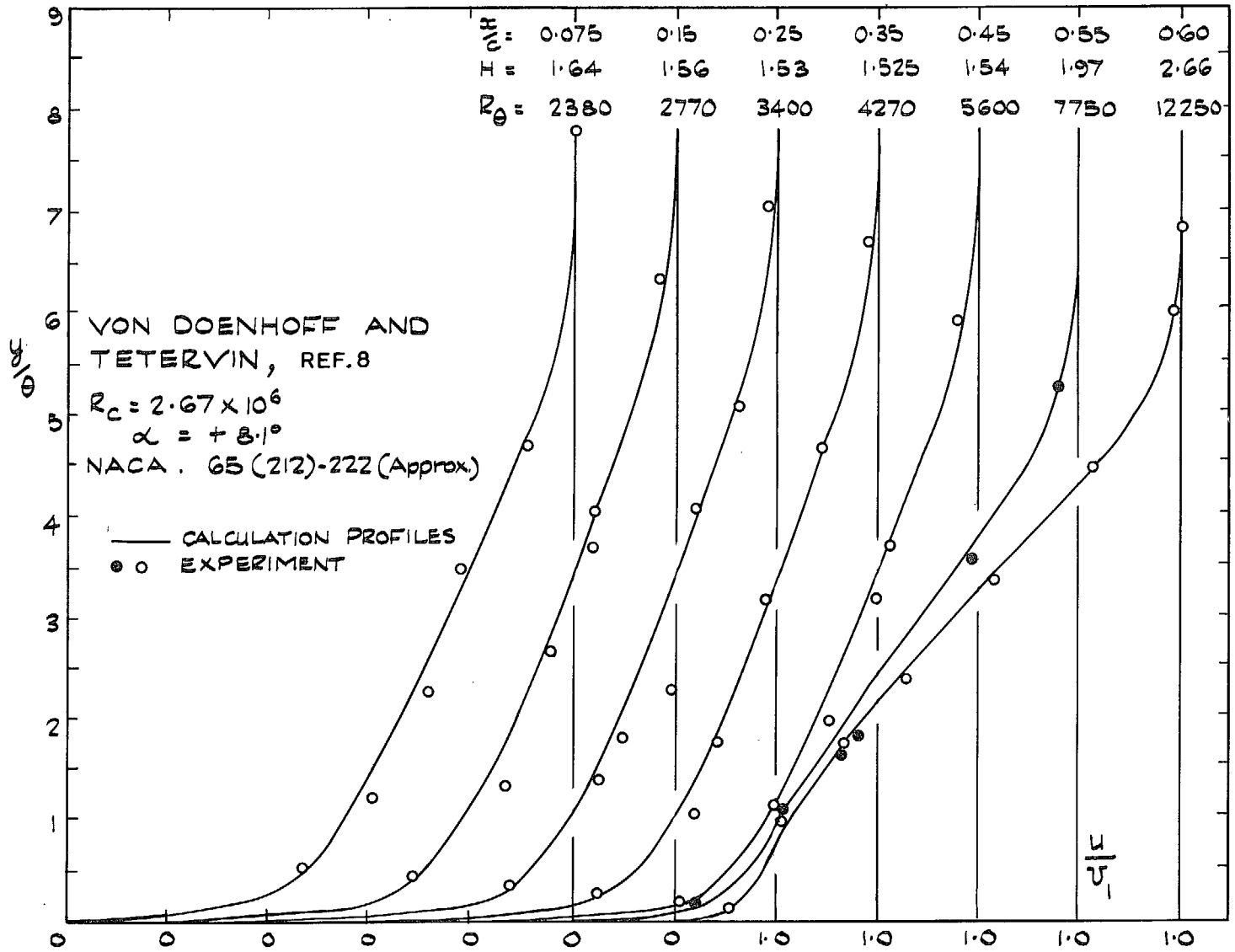

FIG. 19. Comparison of the new family of mean velocity profiles with experiment.

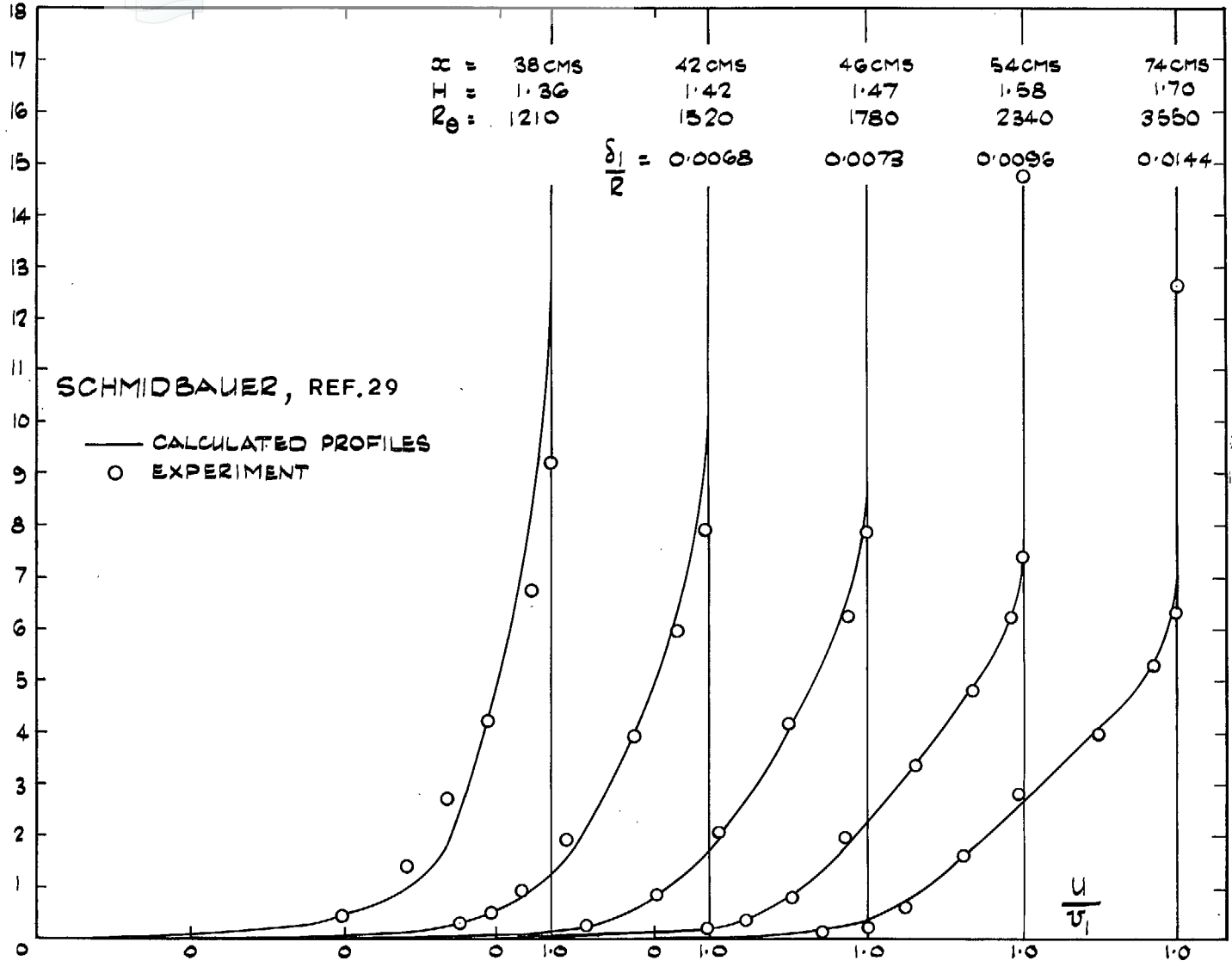

FIG. 20. Comparison of the new family of mean velocity profiles with experiment.

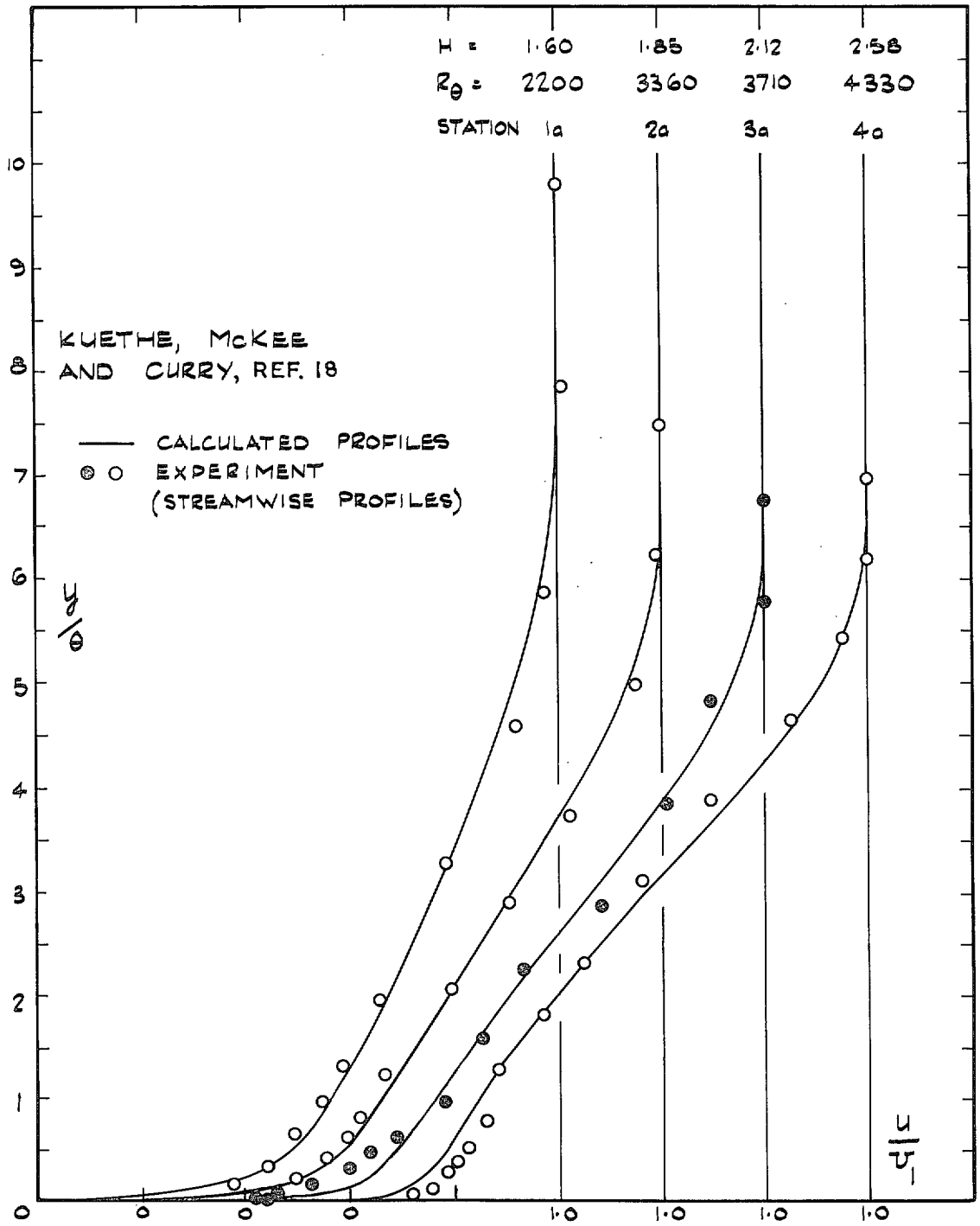

FIG. 21. Comparison of the new family of mean velocity profiles with experiment.

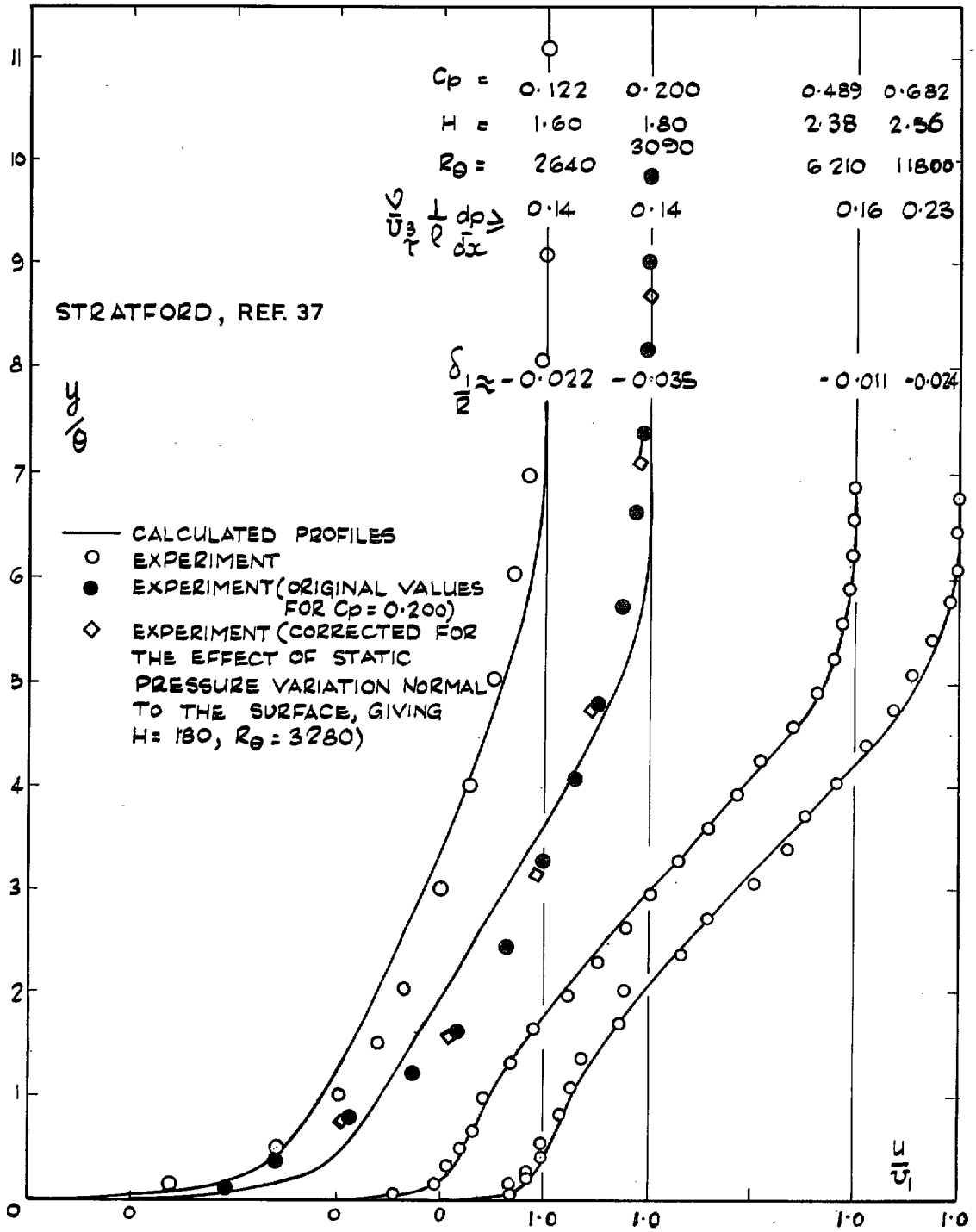

FIG. 22. Comparison of the new family of mean velocity profiles with experiment.

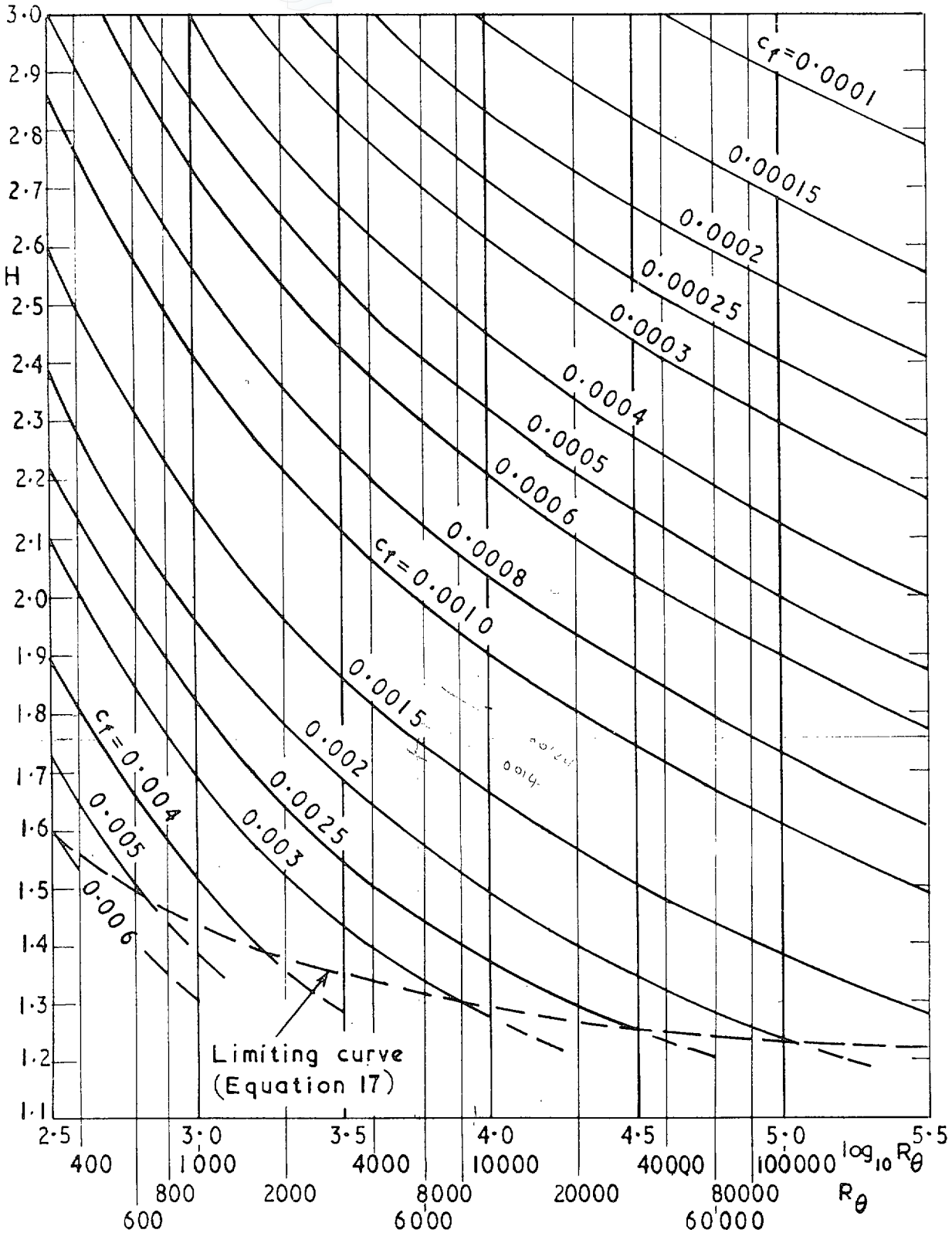

FIG. 23. The new skin-friction law.

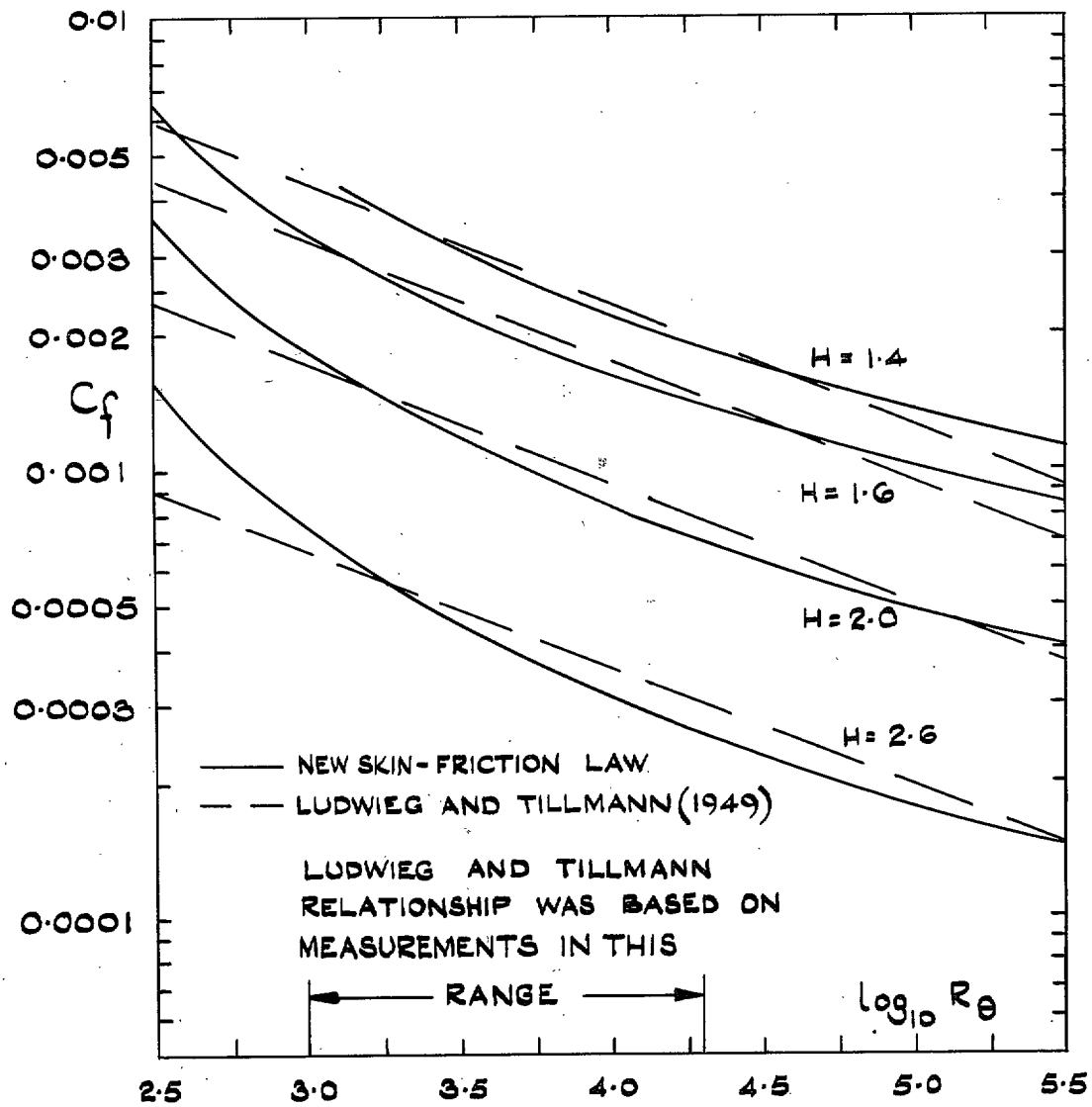

FIG. 24. Comparison of skin-friction laws.

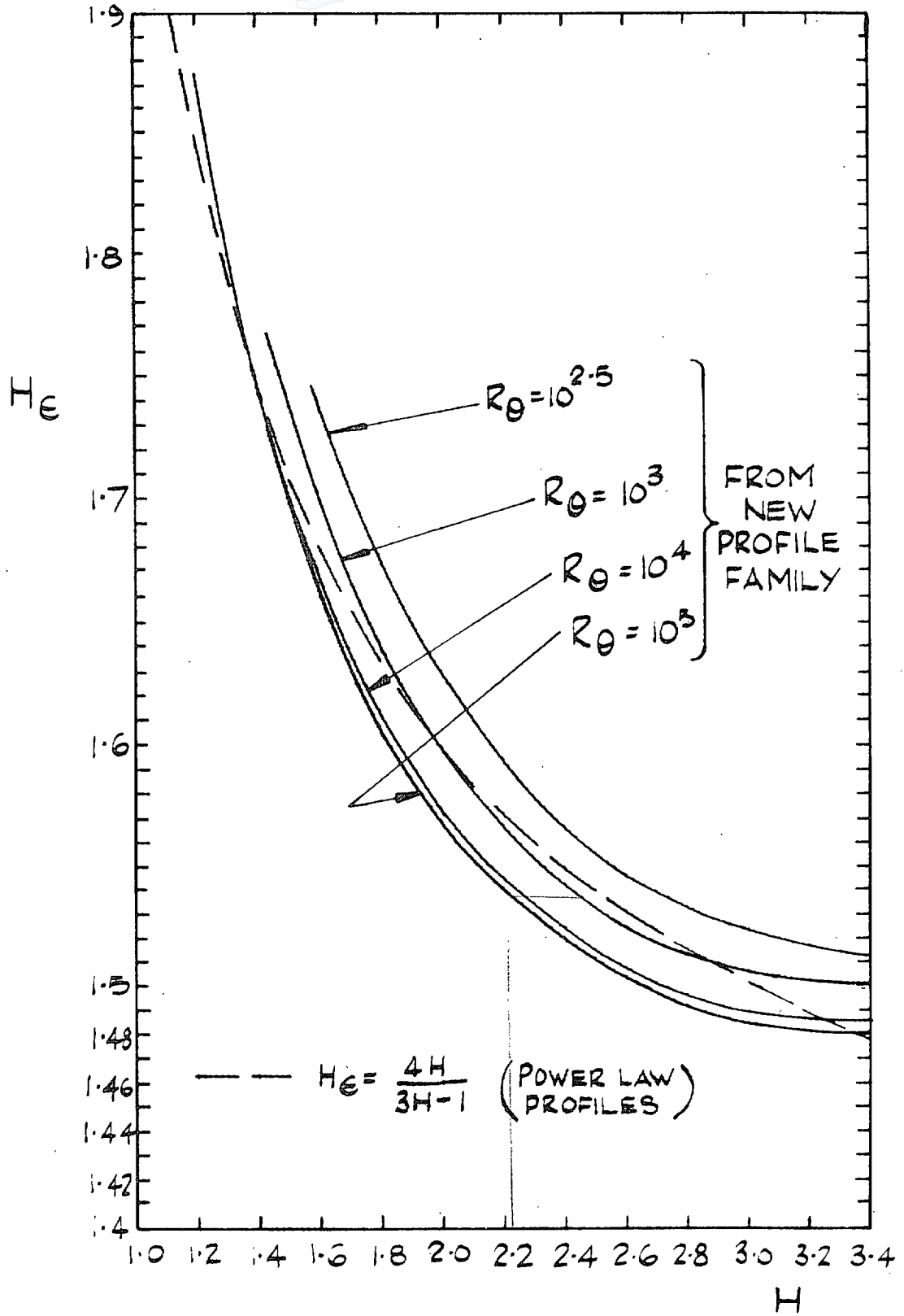

FIG. 25. Comparison of shape-factor relationships.

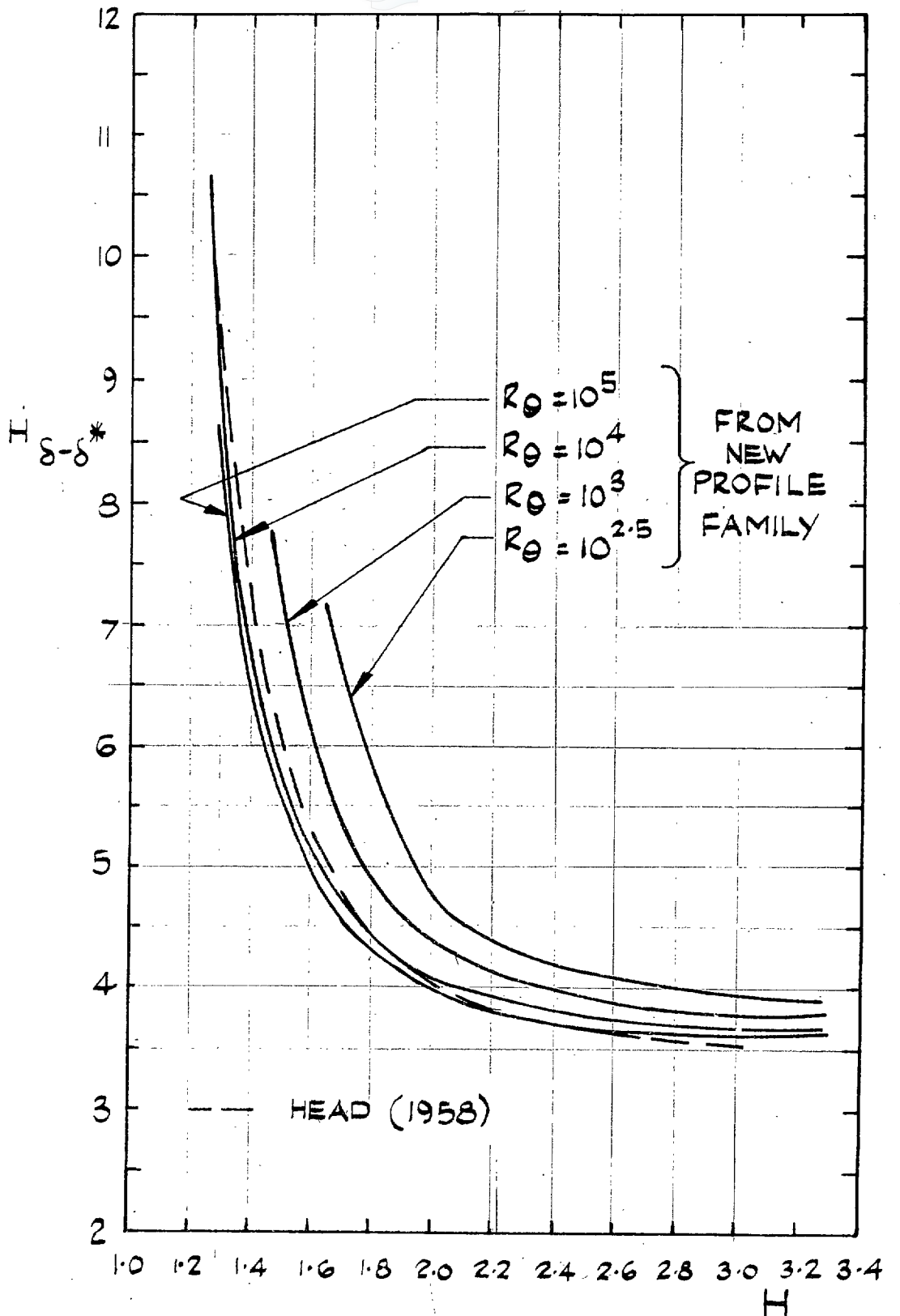

FIG. 26. Comparison of shape-factor relationships.

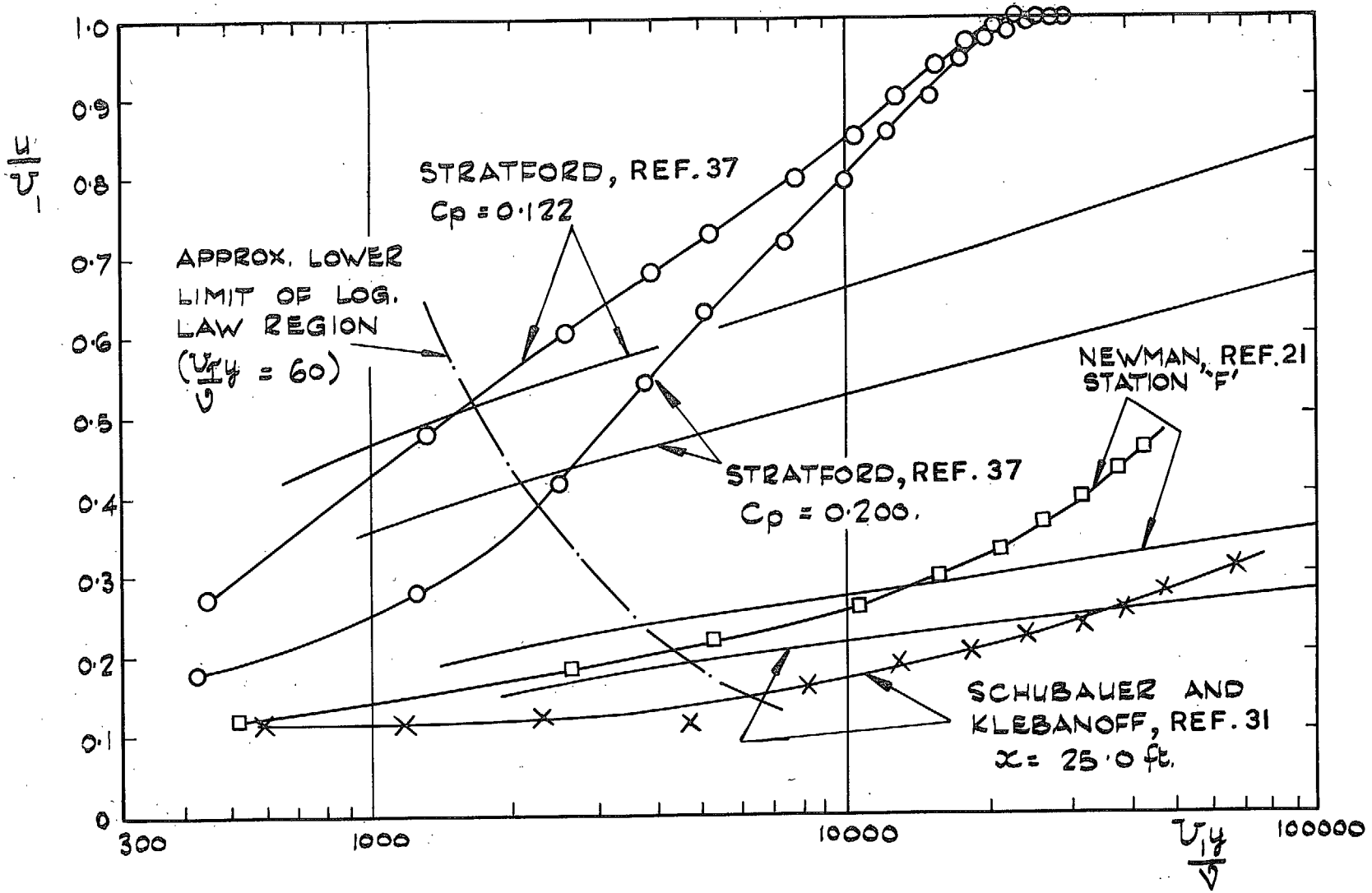

FIG. 27. Comparison of inner region profiles (solid lines corresponding to C_f (H, R_θ) from the new law) with measured profiles for large values of $\frac{\nu}{U_\tau^3}\frac{1}{\rho}\frac{dp}{dx}$ $> 0{\cdot}01$.

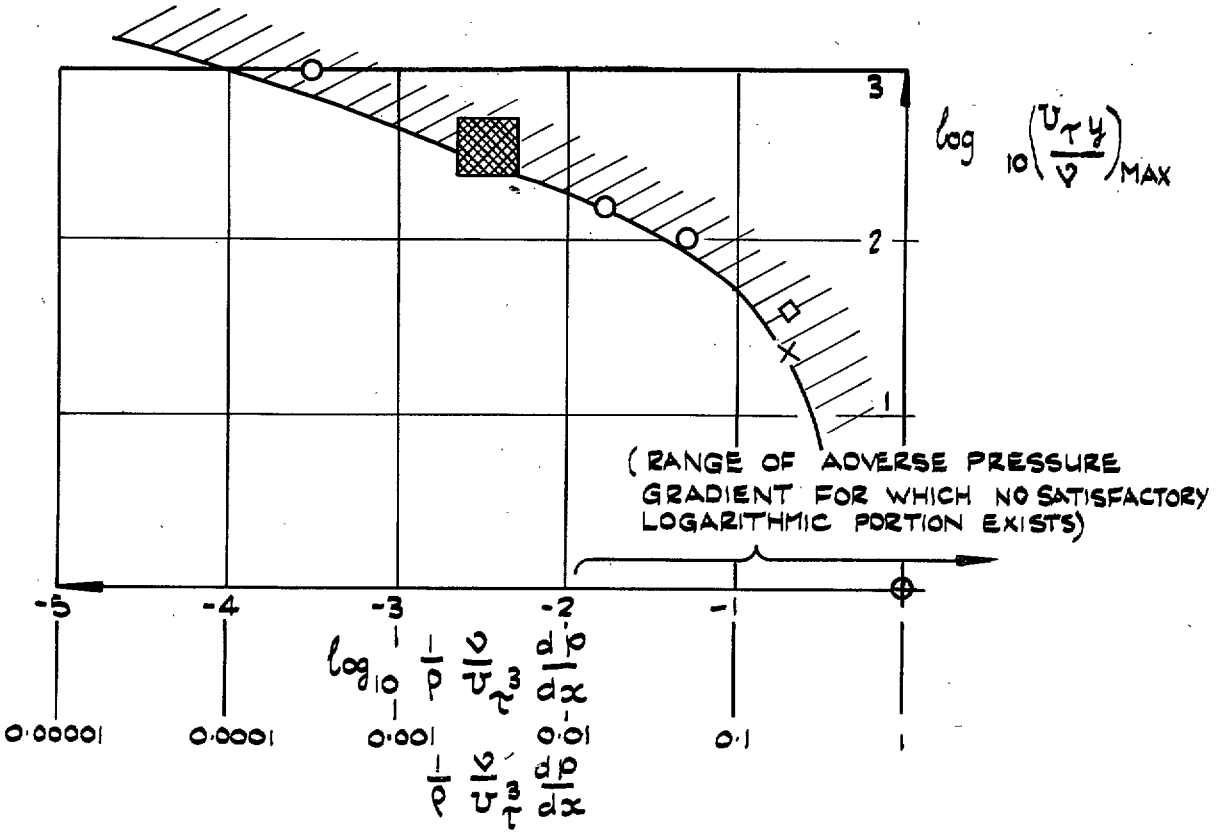

FIG. 28. The estimated effect of adverse pressure gradient on the extent of the 'universal' wall law

(if $y_{max} \leqslant 0{\cdot}1\delta_s$, i.e. $R_{\delta_s}\sqrt{\frac{c_f}{2}} > 1000$)

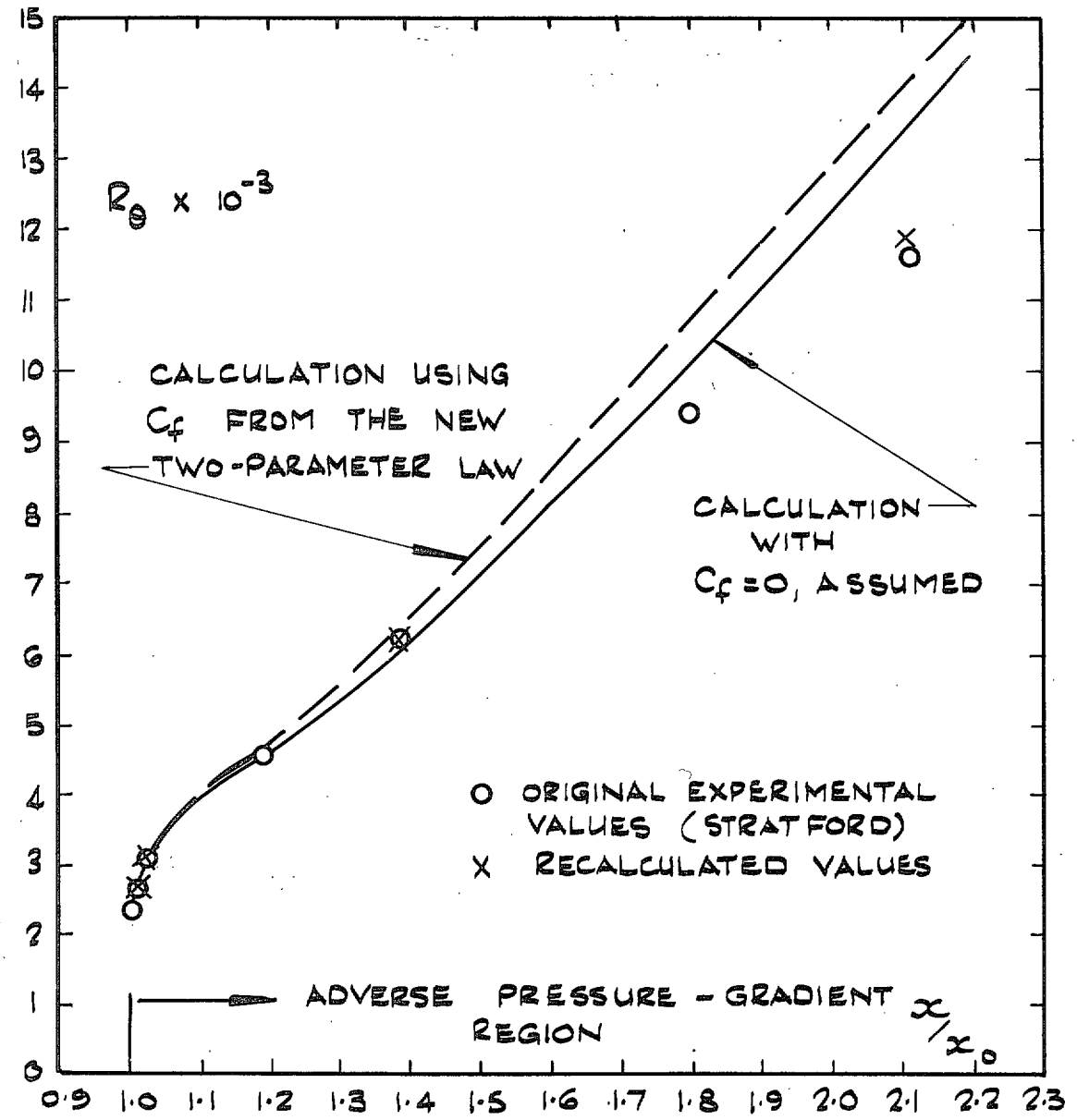

FIG. 29. The effect of skin-friction assumptions on the calculation of momentum development in conditions of strong adverse pressure gradient. [measurements of Stratford[37]]

Printed in Wales for Her Majesty's Stationery Office by Allens Printers (Wales) Limited.

Dd. 129527 K.5.

Published by
HER MAJESTY'S STATIONERY OFFICE

To be purchased from
49 High Holborn, London W.C.1
423 Oxford Street, London W.1
13A Castle Street, Edinburgh 2
109 St. Mary Street, Cardiff
Brazennose Street, Manchester 2
50 Fairfax Street, Bristol 1
35 Smallbrook, Ringway, Birmingham 5
7–11 Linenhall Street, Belfast 2
or through any bookseller

R. & M. No. 3463

S.O. Code No. 23–3463.